Publications of the Astronomical Society of the Pacific
107: 1065–1093, 1995 November

The Photometric Performance and Calibration of WFPC2[1]

JON A. HOLTZMAN,[2] CHRISTOPHER J. BURROWS,[3] STEFANO CASERTANO,[3] J. JEFF HESTER,[4]
JOHN T. TRAUGER,[5] ALAN M. WATSON, [2] AND GUY WORTHEY[6,7]

Received 1995 April 19; accepted 1995 July 26

ABSTRACT. We discuss the photometric performance and calibration of the Wide Field Planetary Camera 2 (WFPC2) on the *Hubble Space Telescope* (*HST*). The stability and accuracy of WFPC2 photometric measurements is discussed, with particular attention given to charge-transfer efficiency (CTE) effects, contamination effects in the ultraviolet (UV), and flat-field accuracy and normalization. Observational data are presented from both WFPC2 observations and ground observations using a system similar to that flown. WFPC2 photometric systems are defined both for the ground and flight systems. Transformations between these systems and the Landolt *UBVRI* system are presented. These transformations are sensitive to details in the spectra being transformed, and these sensitivities are quantified and discussed. On-orbit observations are used to revise the prelaunch estimates of response curves to best match synthetic photometry results with observations, and the accuracy of the resulting synthetic photometry is discussed. Synthetic photometry is used to determine zero points and transformations for all of the flight filters, and also to derive interstellar extinction values for the WFPC2 system. Using stellar interior and atmosphere models, isochrones in the WFPC2 system are calculated and compared with several observations.

1. INTRODUCTION

Accurate understanding of photometric performance and calibration is required to interpret the data from many observations made with the Wide Field Planetary Camera 2 (WFPC2) on the *Hubble Space Telescope* (*HST*). The photometric performance is affected by a small charge-transfer efficiency problem with WFPC2, time-dependent contamination which causes loss of UV throughput, and the accuracy of flat fields. The photometric calibration of the WFPC2 is complicated because the filters used on WFPC2 differ from those used for most ground-based work and because of the premium on *HST* observing time which limits the amount of on-orbit time available for calibration.

The basic procedures for reduction of WFPC2 images and some discussion of instrument performance has been presented by Holtzman et al. (1995, hereafter referred to as H95). The current paper concentrates on issues relevant to photometric performance and calibration.

In astronomy, much photometric work is done with reference to some established standard photometric system. Physical inferences from data are made either from comparison against a large set of observations in this photometric system (e.g., comparison of a color–magnitude diagram against those of globular clusters of known properties) or by using a physical calibration of this system (e.g., determination of cluster ages and metallicities by taking physical stellar models and estimating how physical quantities map into the standard system). Both of these processes require calibration observations, since *a priori* knowledge of absolute responses of telescopes, filters, and detectors is very difficult to obtain accurately.

We consider three ways in which physical information can be drawn from observations with WFPC2. (1) Transform WFPC2 magnitudes onto an already well-studied photometric system and draw physical inferences on the basis of previous work. (2) Accumulate a database of observations in the WFPC2 system and make physical inferences based on comparison with these observations. Most likely, a large reference set of WFPC2 observations of objects about which much is already known will *not* take place with *HST* because of the premium on observing time; however, it is possible to approximate the WFPC2 system from the ground and accumulate data there. (3) Understand the absolute response of WFPC2 and use physical models of the objects being studied. In practice, all of these approaches will be used, and it is important to understand the limitations of each. This paper presents calibration data needed for each of these methods, and estimates the uncertainties with each.

Transformations between observed WFPC2 magnitudes and those on a standard system will depend on the spectral shape of the object being observed; the larger the deviations of the WFPC2 response from that of the standard system, the more sensitive the transformations will be to differences in the underlying spectrum. Because of this, transformations to a standard system will only be accurate to the degree to which the spectrum of the object matches the spectra of the standards used in deriving the transformations. An example of this problem might be that photometric transformations for stars are dependent on the stellar metallicity; if one applies a transformation derived from stars of one composition to stars of a different composition, systematic errors might

[1]Based on observations with the NASA/ESA *Hubble Space Telescope*, obtained at the Space Telescope Science Institute, which is operated by AURA, INC., under NASA Contract No. NAS 5-26555.

[2]Department of Astronomy, New Mexico State University, Box 30001/Dept. 4500, Las Cruces, NM 88003 (holtz@nmsu.edu, awatson@nmsu.edu).
[3]Space Telescope Science Institute, 3700 San Martin Drive, Baltimore, MD 21218, and Astrophysics Division, Space Science Dept., ESA (burrows@stsci.edu, stefano@stsci.edu).
[4]Department of Physics and Astronomy, Arizona State University, Tyler Mall, Tempe, AZ 85287 (jjh@cygloop.la.asu.edu).
[5]Jet Propulsion Laboratory, 4800 Oak Grove Drive, Mail Stop 179-225, Pasadena, CA 91109 (jtt@wfpc2-mail.jpl.nasa.gov).
[6]Department of Astronomy, University of Michigan, Ann Arbor, MI 48109-1090 (worthey@astro.lsa.umich.edu).
[7]Hubble Fellow.

arise. Similar errors might occur for stars with different reddenings. For galaxies, the spectra are composite, so transformations for stars may not be accurate; if the galaxies are redshifted, the spectral differences from zero-redshift stars can be quite large.

An additional complication arises because observations must be made of standards over as wide a range of color as those objects being studied. Because there is a limit to how much time *HST* spends on calibration, observations are *not* made of many individual standards as an observer would do from the ground. Rather, two calibration fields are observed, each of which gives a moderate range of color in a single field. These fields are located in the outer regions of the globular clusters ω Cen and NGC 6752 and were chosen long ago for the original WF/PC (Harris et al. 1993). Some additional data for calibration is available from observations of a few spectrophotometric standards, which are also useful for determining the absolute throughput of the camera. However, all of these data still only sparsely sample the range of stellar colors, metallicities, surface gravities, and reddenings.

To allow a sampling of more diverse stars, we have observed the calibration fields from the ground with a detector and filters which match the flight system as closely as possible. These data are used to determine the differences between the flight and ground photometric systems. We also used the ground system to observe standard stars with a large range of spectral type to determine transformations to a standard system applicable over a broad range of colors. Observations of standard stars also allow us to define a WFPC2 photometric system and set the zero points of the new system to match magnitudes on the standard system for a specified type of star. The ground-based work provides WFPC2 system magnitudes for a set of standard stars, which can be used by observers trying to match the WFPC2 system from the ground.

This procedure was performed for the original WF/PC broadband filters (Harris et al. 1993, 1991; WF/PC Science Verification Report) to get transformations to the Johnson–Cousins *UBVRI* system, as defined by Landolt (1973, 1983, 1992a, 1992b). The accuracy of this photometric calibration was never checked in detail because the errors arising from spherical aberration and limited quality flat fields were large. In addition, the WFPC2 photometric system differs from that of WF/PC because of some different filter bandpasses and because the response of the Loral CCDs in WFPC2 differs significantly from the TI CCDs in WF/PC. Consequently, in this paper we present entirely independent calibration data.

Observations of flux standards on-orbit give us information on how best to adjust the instrument/filter throughputs to match observations. These can then be used for synthetic photometry, and hence for comparison with physical models. Synthetic results can be used to extend transformations to objects with different spectra than the standard stars (e.g., much redder objects, composite spectra, etc.) using spectral libraries or model spectra. They are also important for filters in which we have not obtained ground calibration data.

This paper presents data relevant to the photometric performance and calibration of WFPC2. Section 2 presents data on the photometric performance of WFPC2, including charge-transfer efficiency (CTE) effects, time dependence of throughput in the UV, the accuracy and normalization of flat fields, and aperture corrections. In Secs. 3, 4, and 5, we discuss three related photometric systems: the WFPC2 ground system, defined by observations made with flight spare equipment on the ground; the WFPC2 flight system, defined by observations made on-orbit; and the WFPC2 synthetic system, defined by our best determinations of the absolute throughputs of the flight components. Transformations between the WFPC2 systems and *UBVRI* are also presented. Section 5 uses the synthetic system to determine the physical zero points of the WFPC2 systems, i.e., the conversion from observed count rates to erg cm^2 s^{-1}. Section 6 uses the synthetic system along with model atmospheres to estimate the dependences of transformations on metallicity, gravity, and reddening. Section 7 uses the synthetic system to provide data on extinction and reddening in the WFPC2 system. Section 8 presents a comparison of isochrones in the WFPC2 system with some observations. Section 9 provides a cookbook for photometric calibration which summarizes the use of much of the information presented in this paper.

2. WFPC2 PHOTOMETRIC PERFORMANCE

Before discussing photometric calibration, several issues relating to photometric performance and measurements need to be addressed.

2.1 Charge Transfer Efficiency Effects

The WFPC2 Loral CCDs have a small parallel charge transfer efficiency (CTE) problem which causes some signal to be lost when charge is transferred down the chip during readout. This has the effect of making objects at higher row numbers (more charge transfers) appear fainter than they would if they were at low row numbers. The effect depends on the temperature of the CCDs. At the original temperature of -76 °C, stars in the highest rows could lose as much as 10%–15% of the light within a 0.″5 radius aperture. However, the CCD operating temperature was changed to -88 C on 1994 April 23, and the effect now seems to have a maximum amplitude of ~4% (see H95). These amplitudes were measured from stars with $\gtrsim$1500 total electrons. The brightest stars seem to have a smaller fractional loss, but no large differences are seen in CTE losses for stars in the range 2000 to 20,000 total electrons. Consequently, the effect is not well described by either a constant multiplicative or a constant additive loss per charge transfer. It is possible that losses for fainter stars, at least with no background, may be larger than that quoted above. The problem has been reproduced in the lab, and lab data in conjunction with on-orbit measurements are being used to derive a correction for the effect. The lab data suggest that the magnitude of the problem depends on the amount of background charge on the chip, such that there is significantly less CTE effect in the presence of even a moderate (several dozen electrons) background.

Since a well-tested correction algorithm was not available as of the writing of this paper, we have chosen to make a simple correction to the data used in this paper. All of the frames considered here are short exposures with essentially

no background. For data taken at −88 °C, we have applied a 4% correction ramp to the measured 0.″5 radius aperture photometry, in the sense that we make objects at row 800 brighter by 4%, but do not change the brightness of objects at row 1. This is the correction inferred from dithered observations in ω Cen (H95). It is only an approximate correction because the effect depends on stellar brightness and possibly on the color and the filter because of differences in the shape of the PSF. However, we believe that this correction is accurate to ≲1%–2% for any single observation, and significantly better if many observations spread over the chip are considered. For −76 °C data, we have applied a 12% correction ramp, but we have generally avoided use of −76 °C data wherever possible, and we consider −76 °C data to have larger uncertainties. Our correction is applied to bring measurements to the values they would have in the absence of CTE, or equivalently, the values they would have if measurements were made at row 1. Thus the calibration we derive applies directly to scenes in which CTE is absent (e.g., high background levels), but for scenes with low background, a CTE correction must be applied before using the calibration presented in this paper.

It is possible that, with little background, the wings of stars are more affected by CTE effects than stellar cores. Also, in the wings it is difficult, if not impossible, to correct for CTE losses because of the low signal level. Consequently, photometry using large apertures may suffer more from significant systematic errors than small aperture photometry. These errors could manifest themselves as errors in relative magnitudes of bright and faint stars or as errors in measurements of stars depending on whether there is background present. This effect was considered in our choice of optimum aperture to use for the calibration measurements, discussed in Sec. 2.5.

A lack of a comprehensive understanding of CTE effects probably accounts for the current largest uncertainties for WFPC2 photometry. In particular, we lack direct information about the effect of the CTE problems on very faint stars and on frames with background light. Our current understanding suggests that the CTE problems are caused by electron traps in the CCDs which are filled as charge passes through pixels. However, not all traps are accessible to all electrons passing through: a few traps are only accessible if there is significant charge in the pixel. This model suggests that there will not be significant CTE losses in the presence of background, particularly for faint stars, because background electrons fill the traps before stars pass through the pixels. For brighter stars there may always be a small loss, regardless of the background level. Faint stars in scenes with little background may suffer from larger losses, although the absence of a trend towards larger losses for fainter stars in an intermediate brightness range suggests that this is not necessarily a problem. However, all of this needs to be confirmed from actual observations, and calibration observations to do so have been devised.

2.2 Time Dependence of Throughput

The cold CCD windows slowly accumulate contaminants which degrade the UV throughput. To minimize the degradation, the CCDs are warmed approximately once per month, a procedure which appears to completely remove the contaminants and restore the UV throughput (see H95). To characterize the throughput degradation, observations of a UV-bright flux standard have been taken twice a month through a variety of filters in PC1 and WF3, and roughly twice a week through the F170W filter in all four chips. Four different flux standards have been observed to date: BD +75° 325, AGK +81° 266, Grw +70° 5824, and Feige 110. The first two were only observed early in 1994 when the CCDs were at −76 °C; Grw +70° 5824 was observed at both temperatures, and Feige 110 at −88 °C only.

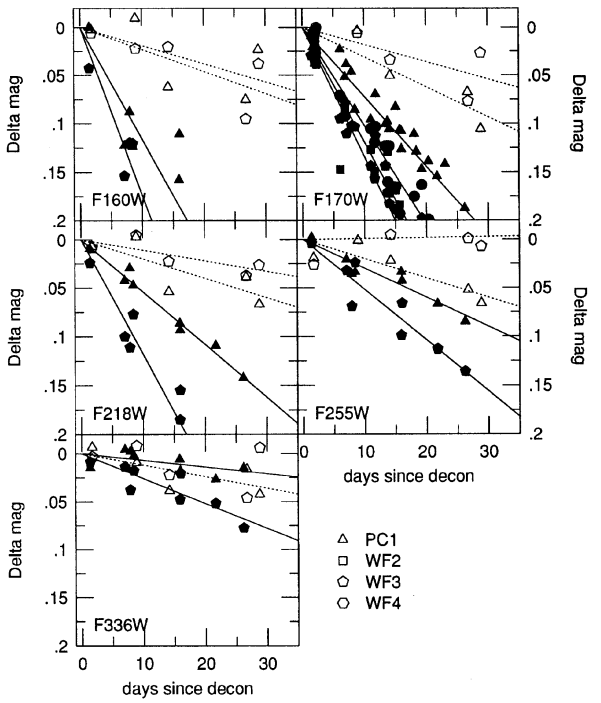

FIG. 1—Time dependence of throughput in the UV. Different panels show throughput degradation in magnitudes since the time of the last decontamination. Different symbols represent the four different chips; filled symbols are for −88 °C data, while open symbols are for −76 °C data. The lines are fits to the data with slopes given in Table 1.

To measure the contamination rate, aperture photometry measurements with an 0.″5 radius aperture were made on all the frames after standard reduction. All of the observations were roughly corrected for CTE effects as discussed above. These data show that the rate of contamination at a given temperature appears to be roughly constant from one decontamination to the next, at least through the first year of observations. Consequently, it is possible to correct for the throughput degradation. The rate of contamination is larger at the current operating temperature of −88 °C than it was at the original −76 °C temperature.

Figure 1 plots the observed count rates in UV filters for the star Grw +70° 5824 as a function of time since the last decontamination. Different symbols represent results for different chips. Open symbols are for −76 °C data, filled symbols are for −88 °C data. For both temperatures, data from several decontamination cycles are plotted.

TABLE 1
Contamination Rates

Filter	Chip	Temperature	Slope
F160W	1	-88	0.0116±0.0005
	3	-88	0.0174±0.0005
	1	-76	0.0019±0.0004
	3	-76	0.0023±0.0004
F170W	1	-88	0.0072±0.0003
	2	-88	0.0119±0.0003
	3	-88	0.0119±0.0003
	4	-88	0.0102±0.0003
	1	-76	0.0031±0.0004
	3	-76	0.0018±0.0004
F218W	1	-88	0.0054±0.0005
	3	-88	0.0118±0.0005
	1	-76	0.0020±0.0004
	3	-76	0.0011±0.0004
F255W	1	-88	0.0030±0.0005
	3	-88	0.0052±0.0005
	1	-76	0.0020±0.0004
	3	-76	-0.0001±0.0004
F336W	1	-88	0.0007±0.0005
	3	-88	0.0026±0.0005
	1	-76	0.0012±0.0004
	3	-76	0.0007±0.0004

Figure 1 shows there is significant degradation in throughput at all UV wavelengths. The rate of degradation differs from chip to chip and at the two different CCD temperatures. Table 1 presents fits for the degradation of the form:

$$m(\text{obs}) = m(\text{true}) + d \times t, \quad (1)$$

where $m = -2.5 \times \log(\text{DN s}^{-1})$ is the instrumental magnitude, d gives the contamination rate, and t is the time in days since the last decontamination. A list of decontamination data was presented in H95 and can be obtained from the STScI. These fits can be used to roughly correct observed count rates in the UV. The degradation is wavelength dependent, so the true correction is probably a function of the spectrum of the observed object; the degradations presented here were measured from observations of hot stars.

It is clear that the contamination rate depends on which camera is being used. Most likely there are also variations across the field of each individual chip. Analysis of internal flat-field data suggests that the relative variations within each chip are roughly a factor of 3–5 lower than the absolute variation of the throughput as compared with an "uncontaminated" state (H95), implying variations of up to 10%–20% across a chip at the shortest wavelengths after 30 days. The chip dependence of throughput degradation has only been measured for all four chips in F170W; for the other filters, only PC1 and WF3 were monitored. If we assume that the relative variation between the chips is independent of wavelength, we can estimate the degradation rates for all filters in WF2 and WF4. Based on the F170W data, we estimate that the rate of contamination in WF2 is roughly equal to that in WF3, and that the rate of contamination in WF4 is roughly 1.5 that of PC1. Clearly, these are just estimates, but it is likely that these rough corrections can bring most individual UV measurements within a few percent of their "true" values.

Several UV filters (F122M, F185W, and F300W) were not part of the monitoring program and thus we have no direct data with which we can estimate contamination. However, the throughput degradation appears to decrease monotonically with wavelength, so at least for F185W and F300W, rough contamination rates can be inferred by interpolating between observed values in other filters. For F122M, the situation is more uncertain.

At longer wavelengths, no obvious trends with time are observed, implying that contamination above 4000 Å is less than can be easily measured. However, there is some indication that there is contamination which can affect visible throughput by as much as a few percent in WF3 (see the WFPC2 Instrument Handbook, Version 3.0); no such effects are seen in PC1, although it is likely that throughput degradation at the sub-percent level is present.

The operating temperatures of the WFPC2 CCDs were changed on 1994 April 23 from −76 to −88 °C. This was motivated by the charge-transfer efficiency problem and by a significant growth rate of hot pixels at −76 °C (H95). The temperature change improved both of these problems. However, the temperature change also probably changed the QE of the detectors in the near IR. The exact change is difficult to measure because of the concurrent change in CTE properties, but we estimate that the QE through F814W was higher by ~5% (H95) at −76 °C. At F555W, we believe there was little change in the QE with the change in temperature; at intermediate wavelengths between 6000 and 8000 Å, there was probably a few percent change.

2.3 Flat Fields

To get accurate count rates which are independent of field position, flat fields must be applied to the data before photometric measurements are made. Observed count rates after flat fielding depend on the normalization of the flats. For all data presented in this paper, the flat fields installed in the STScI pipeline in 1994 March were used. The construction of these flats is described in H95. All flats were normalized to have a mean value of unity in the region (200:600,200:600) in WF3. The other chips should be properly cross-normalized to reflect any true differences in sensitivity or gain between the chips (which are generally small). As discussed in H95, the flats in the visible region of the spectrum are expected to be good to within 1% on small scales, and within a few percent on large scales. Flats for the UV filters probably have larger errors.

All flats were constructed using data from the gain=14 (electronics bay 3) channel. The exact values of the gain differ from chip to chip as described in the WFPC2 Instrument Handbook or the WFPC2 Science Calibration report. However, for count rates in DN, differences in the gain between chips are removed by flat fielding. A flat-fielded image taken with bay 3 of a uniform source will have the same count rate in DN s^{-1} in all chips even if the actual gain

values vary slightly from chip to chip, and it will have approximately half the count rate of the same source taken with gain=7 (bay 4). The noise characteristics will be slightly different from chip to chip, but since the gain values are all very close to each other, these differences are negligible. Flat fielding of images taken with bay 4 is discussed in Sec. 2.4.

Comparisons of the observed count rates for the spectrophotometric standards on each chip after flat fielding provide an estimate of the accuracy of the chip-to-chip normalization of the flats. In most of the visible wavelength filters, the agreement between flat-fielded data in PC1 and WF3 is good, typically within two percent, although at the longest wavelengths, there is evidence for chip-to-chip normalization errors reaching nearly five percent. However, the data are limited and this result has not been confirmed.

In the UV, the situation is worse. In F170W, data from all four chips have been compared, and there are deviations of tens of percent between the observations in different chips, even for observations taken immediately after decontaminations. Variations of this amplitude are not seen in the thermal vacuum (TV) test data which were used to construct the on-orbit flat fields. Data from PC1 and WF3 in other UV filters also show significant discrepancies. These chip-to-chip differences are currently not well understood. Some of the UV filters have significant red leak which can be field dependent, but TV data suggests that this is not the problem for F170W. Also, red leak is not expected to contribute a significant amount of counts for the blue stars considered here. One possibility is that permanent contaminants were deposited at some time since TV onto the internal WFPC2 mirrors, with different degrees of contamination on the optics for each camera. Another possibility is variations in camera throughput at the shortest wavelengths in a filter, where the flux standards provide maximum count rates, as opposed to the longest wavelengths in the filter which may dominate the UV light in the flat fields, though even if this is the case, it is hard to understand variations as large as those seen.

If modifications are made to flat fields in the future, they may affect the calibration results presented in this paper since photometric zero points are tied to the normalization of the flat fields. We suggest that if such modifications are made, the normalization should be set the same as the current flat fields; if so, any changes to the photometric calibration data should be small.

2.3.1 Geometric distortion and flat fields

Because the WFPC2 cameras have geometric distortion, the effective pixel sizes vary across the field of view, both within the field of view of each camera, and also between the different cameras. Application of flat fields corrects for the change in pixel size among all of the WF cameras, because less light falls in pixels with smaller areas. Consequently, application of flat fields normalizes all WF pixels to have the same area. In this process, surface brightnesses are correctly preserved, but integrated photometry is corrupted (see discussion in H95). Observers who want to measure total brightnesses, as opposed to surface brightnesses, need to correct measurements made on flat-fielded images for the change in pixel size across the field; measurements should be multiplied by the ratio of the true pixel area to the normalized area. The maximum correction reaches about 5% in the corners of the images. In addition, the scale varies very slightly between the different WF cameras, so there is a very small camera-to-camera correction to get correct integrated brightnesses between chips. We have chosen the center of WF3 to define the nominal pixel area for our photometric calibration.

For the PC, an approximate correction for the different pixel areas has been incorporated into the flat fields. Observed flats in the PC have been multiplied by the ratio of the design focal ratios, $(28.3/12.9)^2$, so that the values in the flat fields are close to unity. Thus, in the PC, an approximate correction has been made to preserve integrated brightnesses, but surface brightnesses will not directly match the WF cameras; e.g., after flat fielding, the sky level is significantly lower in the PC. To match surface brightnesses per pixel between the PC and the WF chips, the PC frames should be multiplied by $(28.3/12.9)^2$. There is distortion within the PC camera which causes a variation of pixel area within the PC chip, but this variation *is* removed by flat fielding. To match integrated brightnesses between the PC and the WFs, one needs to multiply by the ratio of the true pixel areas to the design value.

In summary, if one wishes to measure surface brightness, use the flat-fielded images but multiply the PC by $(28.3/12.9)^2$; use the WF3 pixel scale. If one wishes to measure integrated brightness, measurements on flat-fielded images must be corrected for the normalization of pixel areas. This correction includes a factor for the variation in pixel size within each camera, then an additional factor to normalize all cameras to the same pixel area. For the internal camera correction, maps of the pixel areas relative to the center of each chip were presented in H95. To normalize all measurements to the center of WF3, measurements from (the center of) each chip need to be multiplied by 1.0066, 1.0005, 1., and 1.0013 for PC1-WF4; the PC factor has already included the rough normalization built into the flat fields.

The WFPC2 CCDs also have the feature that every ~34th row has a slightly lower sensitivity. It has not been conclusively determined whether this is a geometric effect (smaller pixels) or not. However, even if it is, removing it by flat fielding will introduce <1% error for integrated photometry of a point source.

2.4 WFPC2 Gain States

WFPC2 can be read out through either of two gain states with approximate gains of 14 e^-/DN (bay 3) and 7 e^-/DN (bay 4). The same flat fields (with the same normalization) are currently used for data in either gain state. Since all of the photometric calibration data are taken with bay 3 (gain =14), it is important to know the ratio of the two gains accurately to use the calibration for bay 4 (gain=7) data. This ratio was derived from observations of a stable and monitored light source made during TV. These data show a slightly different gain ratio for each of the four chips; this is not unexpected because there are some electronics in each bay that are separate for each chip, even though the A/D converters in each bay are common to all four chips. The TV

data give count ratios (bay 4/bay 3) of 1.987, 2.003, 2.006, and 1.955 for PC1, WF2, WF3, and WF4, respectively. Similar chip-to-chip ratios are found in on-orbit internal flats, though the absolute ratio is lower in all chips by 1%–2%. However, the absolute value of the ratio is more uncertain for the internal flat data which are taken with a lamp that may vary in intensity. A similar difference in gain ratios from chip to chip is also indicated by some stellar data. These data suggest a value for the absolute ratios which is slightly higher (~1%) than the values determined in TV.

Because the flat fields were derived from bay 3 data, there will be no differences in count rates between the chips for flat-fielded bay 3 data. However, for bay 4 data, the current flat fields will leave small differences in count rates between the chips.

For the current paper, calibration for the different gains is parametrized by the gain ratio, GR_i, defined as the ratio of the counts of a source using bay 4 to the counts using bay 3. The subscript gives the chip number. GR_i is unity for all chips in bay 3 because the flats were constructed from bay 3 data. For bay 4, the TV observations discussed above suggest the values 1.987, 2.003, 2.006, and 1.955. These values probably are uncertain by ~1%, leading directly to possible ~1% systematic errors in photometry for bay 4 data. It is possible that the bay 4 flats will be renormalized to reflect the bay 4 gain differences between chips; if this is done, then the values which should be used for GR_i will be changed (presumably to some constant value).

2.5 Aperture Corrections

The point-spread function (PSF) for a diffraction limited image has extensive low-level wings, and scattering from small-scale structure and dust on the *HST*/WFPC2 mirrors contributes additional light to the wings of the PSF. In discussing photometric calibration, it is important to reference the photometric measurements to some aperture size.

In ground-based work, photometric measurements are typically extrapolated to "infinite" radius using observations of bright stars. This extrapolation is required if one wishes to use observations of stars to calibrate surface photometry of extended sources, although surface photometry is still only perfectly accurate in the limit of a uniform extended source.

For WFPC2, measuring corrections to "infinite" aperture is complicated by the small pixel size and extended PSF wings which require extremely accurate background values for good large-aperture measurements, the digitization effects of the WFPC2 A/D converters, and the CTE problems which may make observed aperture corrections dependent on the amount of background in the frame.

To minimize these problems we have chosen to use an intermediate-sized aperture of 0.″5 radius for all of the photometric calibration measurements. For an aperture of this size, CTE effects are likely to be correctable to within ~1%–2% for all of the stars considered here (which are relatively bright) using the simple algorithm discussed in Sec. 2.1. In addition, observers can correct point-source photometry to this aperture size without complications arising from extrapolating to a larger aperture. Such extrapolations can be difficult, especially in a crowded field. Consequently, calibration of photometry of point sources using the data presented herein should be spared some of the possible systematic errors which arise when using larger apertures.

For observers who wish to do surface photometry, the results presented here can be extrapolated to larger (or infinite) aperture size, although the inherent uncertainties in doing so must be incorporated into estimates of possible systematic errors. Encircled energy curves, from which aperture corrections can be derived, are presented in H95 for data in which there is little background. These curves should apply to the data presented in this paper, which were all taken with little background. We find that roughly 90% (less in the UV) of the total light is contained within a 0.″5 radius. A discussion of scattering in the WFPC2 and a presentation of a PSF that may be more applicable to situations in which there is background is presented by Krist and Burrows (1994).

We note that photometry using apertures smaller than our nominal 1″ diameter is subject to a different set of possible systematic errors. For small apertures, the observed flux depends on details of the PSF such as pixel centering, small focus variations, variations in the PSF as a function of field location, and telescope jitter during exposures. From the set of observations of spectrophotometric standards and from models of the *HST*/WFPC2 PSF, we have inferred that such effects almost always give $\lesssim$1% errors using our nominal aperture size (H95). The errors are larger for smaller apertures, so observers using smaller apertures are cautioned that they should derive separate aperture corrections for each frame on which measurements are made.

Aperture photometry also depends on how the sky is determined. Usually, the sky level is measured by taking a modal or median value in a region away from the object in question. Since the wings of the WFPC2 PSF extend out a long way, one needs to choose a region far from the object in order to measure a true sky value. For all of the WFPC2 measurements presented here, we have chosen a sky annulus from 4 to 6 arcseconds from each object. In practice, observers often choose a smaller annulus; a smaller annulus will include more light from the wings of the star, so all sky-subtracted measurements will be lower. Given a stable PSF, it is possible to determine the correction for a measurement with an arbitrary choice of sky annulus to correct it for the "true" sky value; such estimates can be made using the data from H95 and Krist and Burrows (1994). We have chosen to use a "true" sky value because its meaning is clear and because some techniques (e.g., profile-fitting photometry) make measurements while attempting to derive an absolute sky value.

3. THE WFPC2 GROUND PHOTOMETRIC SYSTEM

We now begin the discussion of photometric calibration. In this section, we discuss the WFPC2 ground photometric system, which is needed to derive accurate transformations to *UBVRI* and to define zero points for the WFPC2 flight system. Section 4 will present the WFPC2 flight system and how it relates to the WFPC2 ground system and to *UBVRI*.

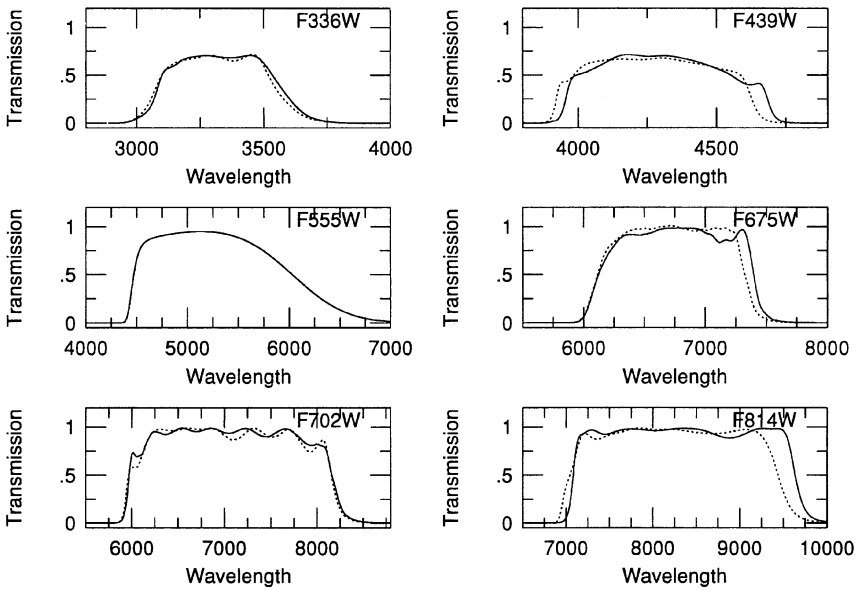

FIG. 2—Filter response curves for several flight filters (solid lines) and the corresponding flight spares (dotted lines) which were used in the SSO observations.

3.1 Observations

Observations were made of many standard stars and the flight calibration fields during 1994 April with the 1-m telescope at the Siding Springs Observatory (SSO). A lumogen-coated Loral 800×800 CCD from the same lot as the flight chips was used. This chip did not have a MgF window as the flight packages do, and the dewar had a quartz window on it. However, both MgF and quartz have very flat response across the visible part of the spectrum so these differences are not expected to change the response significantly. The dewar was mounted directly at the Cassegrain focus of the 1-m telescope. Consequently, there were only two reflections in the system (from the telescope), compared with seven reflections for the WFPC2 on-orbit (because there are five reflections within the WFPC2). The CCD was operated in 2×2 binned mode to increase observing efficiency; in this mode, the $f/8$ system gave ~0.″75/pixel.

Observations were made using the following filters: F336W, F439W, F555W, F675W, F702W, and F814W. Although these were flight spare filters, there are small differences in the measured passbands as compared to the flight filters. Figure 2 shows lab measurements for both the flight (solid curves) and ground (dotted curves) filter passbands for the six filters.

The observing run lasted for eight nights from 1994 April 15 to April 22. On each night, observations were made using five of the six flight filters. Flat fields of the evening and morning twilight sky were taken. A separate flat field was constructed for each night. Flats from each night were compared and the agreement was very good except that a few pieces of dust fell onto the CCD window during the run, adding a few low-level features to the flats for the later nights; because of these, a separate flat was used for each night. Bias frames were also taken daily, but no differences were seen during the course of the run, so all of the bias frames were combined to make a single superbias frame for the run. Standard reduction consisted of overscan subtraction, superbias subtraction, and flat fielding.

The seeing provided ~2″ images for the first half of the run, but the image size improved to 1.″25–1.″5 for the last half of the run. Three of the eight nights were judged to be photometric from the scatter in the standard star transformations and in repeat observations. Fortunately, these photometric nights were the last three nights of the run, when the seeing was also the best.

3.2 Standard Stars and Definition of the WFPC2 Ground System

On each night, observations of between 50 and 100 standard stars were made. These were taken from the compilations of Landolt (1983, 1992a, 1992b), and included both single star fields as well as fields with several standards. The Landolt standards were measured using aperture photometry, using an aperture of diameter ~22.″5.

The response of the ground system defines the WFPC2 ground photometric system. To get magnitudes on this system for the standard stars, we need to make corrections for atmospheric extinction and to define zero points for the new system. For zero points, we have chosen to make stars with zero color on the *UBVRI* system have zero color on the WFPC2 system (although see below). The magnitudes in each bandpass are defined so that a star of color zero has WFPC2 magnitudes equal to the *UBVRI* magnitudes. The physical fluxes corresponding to a WFPC2 magnitude are then the same as those for the *UBVRI* magnitude for a star of color zero. In practice, we do not observe stars with a color of exactly zero, so the zero points are set by looking at the locus of standard stars and determining a zero point from a fit of magnitude versus color. This also provides transformations between the WFPC2 system and the *UBVRI* system.

The transformations between the WFPC2 system and *UBVRI* for stars of zero color are sensitive to the surface gravity of the observed objects because the WFPC2 passbands differ significantly from the *UBVRI* passbands. Because of this, all stars of zero *UBVRI* color will not have zero WFPC2 color. Practically, the WFPC2 ground system is defined to have zero points which match *UBVRI* magnitudes for the stars near color zero which we observed with the ground system. Since it is not possible to observe bright stars with the CCD system, the stars around color zero which were observed are typically white dwarfs, not main-sequence stars. So, in fact, our zero points match WFPC2 magnitudes to *UBVRI* magnitudes for stars of color zero with high surface gravity. For main-sequence stars of color zero, the WFPC2 ground magnitudes would not match the *UBVRI* magnitudes; Vega, for example, would not have its standard *UBVRI* values on the WFPC2 ground system. The difference between WFPC2 magnitudes for these stars and for main-sequence stars can be determined from synthetic photometry and will be discussed in Sec. 6. Anticipating these results, we find that the zero points would change by $<2\%$ for F555W, F675W, and F814W, by $\sim 3\%$–5% for F439W, and by more for F336W if we were to reference the ground WFPC2 system to main-sequence stars of color zero. For stars of zero color, higher surface-gravity stars have less flux through F439W and F555W (more flux through F336W) than lower surface-gravity stars. Consequently, observations of main-sequence stars of color zero will have WFPC2 magnitudes which are fainter than the *UBVRI* magnitudes in F439W and F555W. Since we infer these differences from models, not observations, we have chosen to leave the WFPC2 ground-system definition to match the observed stars. The comparison of synthetic zeropoints (which are normalized to Vega) and observed zero points (normalized to white dwarfs) which will be presented in Sec. 5 quantifies the difference in zero points.

The reduction of the standards was accomplished as follows. First, we determined instrumental magnitudes (corrected for extinction) and first and second-order extinction coefficients. We iteratively solved for these quantities using the definition:

$$I_{ij}=-2.5\times\log c_{ijk}+k_{1in}\times X_{ijk}+K_{2i}\times X_{ijk}\times(I_{\mathrm{F555W},j}-I_{\mathrm{F814W},j}) \tag{2}$$

where I are the instrumental magnitudes, c the observed count rates, k_1 and K_2 are first- and second-order extinction coefficients, and X is the airmass. The subscript i represents the six different filters, the subscript j represents the approximately 50 different stars observed, the subscript k represents multiple observations of a given star through a given filter, and the subscript n represents the three different nights. We solved for the set of several dozen instrumental magnitudes plus extinction coefficients for each filter for each of the three nights using a least-squares fit to all of the available data. All of these quantities were determined simultaneously and iteratively because of the presence of the instrumental (F555W–F814W) in the second-order extinction term; the solution converged within five iterations.

Because we had limited data for stars of different colors at different airmasses, we had difficulty in accurately solving for second-order extinction coefficients. We determined starting guesses for the second-order extinction terms using synthetic photometry on the Bruzual, Persson, Gunn, and Stryker (BPGS) stellar atlas using estimates for the response of the different elements in the system and an atmospheric extinction curve from Lockwood (private communication). In the fits, we constrained the second-order coefficients to be the same for all three nights, unlike the first-order coefficients which were allowed to vary from night to night. We adopted the derived second-order coefficients when they lowered the reduced χ^2 of the fit as compared to when we left the coefficients locked at the synthetic values. This procedure gave us derived second-order coefficients for F336W and F439W, but for the other filters, the synthetic values were adopted.

Given the instrumental magnitudes, we then determined zero points for the WFPC2 ground system by solving:

$$U_j=I_{\mathrm{F336W},j}+T_{1,\mathrm{F336W}}\times(U-B)+T_{2,\mathrm{F336W}}\times(U-B)^2+Z_{\mathrm{F336W}}, \tag{3a}$$

$$B_j=I_{\mathrm{F439W},j}+T_{1,\mathrm{F439W}}\times(B-V)+T_{2,\mathrm{F439W}}\times(B-V)^2+Z_{\mathrm{F439W}}, \tag{3b}$$

$$V_j=I_{\mathrm{F555W},j}+T_{1,\mathrm{F555W}}\times(V-I)+T_{2,\mathrm{F555W}}\times(V-I)^2+Z_{\mathrm{F555W}}, \tag{3c}$$

$$R_j=I_{\mathrm{F675W},j}+T_{1,\mathrm{F675W}}\times(V-R)+T_{2,\mathrm{F675W}}\times(V-R)^2+Z_{\mathrm{F675W}}, \tag{3d}$$

$$R_j=I_{\mathrm{F702W},j}+T_{1,\mathrm{F702W}}\times(V-R)+T_{2,\mathrm{F702W}}\times(V-R)^2+Z_{\mathrm{F702W}}, \tag{3e}$$

$$I_j=I_{\mathrm{F814W},j}+T_{1,\mathrm{F814W}}\times(V-I)+T_{2,\mathrm{F814W}}\times(V-I)^2+Z_{\mathrm{F814W}}, \tag{3f}$$

where *UBVRI* are the standard values from Landolt (1983, 1992a, 1992b), T_1 and T_2 are the first- and second-order transformation coefficients, and again, the solutions were done using least squares. We then define the WFPC2 ground-system magnitudes to be the instrumental magnitudes plus the zero points. We adjusted the extinction coefficients to take account of the zero point shift in (F555W–F814W) so that, finally, the ground-system magnitudes can be written:

$$M_{ij}=I_{ij}+Z_i=-2.5\times\log c_{ij}+K_{1in}\times X_{ijk}+K_{2i}\times X_{ijk}\times(M_{\mathrm{F555W}}-M_{\mathrm{F814W}})+Z_i, \tag{4}$$

where M are the ground-system magnitudes, and $K_{1in}=k_{1in}-K_{2i}\times(Z_{\mathrm{F555W}}-Z_{\mathrm{F814W}})$. The final extinction coefficients are presented in Table 2; both the synthetic and derived second-order coefficients are presented to give a feeling for the differences.

This method of determining zero points works only if the transformation between the WFPC2 ground system and the *UBVRI* system is well represented by a second-order relation in stellar color. We found that this was accurate representation for all of our filters except for F336W. F336W is complicated for two separate reasons. First, the filter has a red

TABLE 2
Extinction Coefficients for SSO observations

Filter	K_1(4/20)	K_1(4/21)	K_1(4/22)	K_2	K_2(syn)	K_2(fit)
F336W	−0.841	−0.904	···	0.185	0.058	0.185
F439W	−0.321	−0.358	−0.335	0.043	0.015	0.043
F555W	−0.162	−0.187	−0.169	0.010	0.010	0.013
F675W	−0.107	···	−0.115	0.002	0.002	-0.009
F702W	···	−0.123	−0.113	0.005	0.005	0.014
F814W	−0.079	−0.102	−0.093	0.002	0.002	0.007

leak which is significant even for moderately red objects. Second, the F336W bandpass differs significantly from the U bandpass: the F336W bandpass falls shortward of the Balmer discontinuity, while the U filter straddles it. This causes deviations from a quadratic relation for stars with a Balmer discontinuity, and in fact the F336W-U relation is multivalued in this region. These effects are shown in Fig. 3, which gives a synthetic estimate of the difference between U and F336W and also the red-leak contribution (defined as all light coming from λ>4000 Å) as a function of stellar color, using throughput estimates and the BPGS library of stellar spectra. The multivalued region around $U-B=0$ is apparent. Based on the red-leak data, we restricted our fit for extinction to stars with $V-I<1.0$. In determining the zero point for F336W, we restricted the fit to stars with $U-B<-0.1$, because the synthetic results show that the relation between F336W and U should be well represented by a quadratic function in this color regime.

Because of the limited number of observations of each star, the WFPC2 ground magnitudes for each individual stars have not been determined to the accuracy usually obtained for standard stars. Photon statistics limit the accuracy of each observation to a few millimag, but the true errors are larger, typically 1%–2%, mostly because of possible errors in the determination of the extinction coefficients. Because of the large number of stars observed, we feel that we have adequately defined the system. However, it is likely that observers will want a set of WFPC2 standard stars which can be observed from the ground so that they can use a flight-like system to calibrate on-orbit observations. The limited accuracy of individual measurements, as well as the restricted sky coverage, limits the usefulness of the standard magnitudes measured here for this purpose. However, we are currently undertaking observations of Landolt equatorial standards around the sky using the same filters and detector at Lowell Observatory. We will use the overlap of stars observed both at Lowell and at SSO to determine if there is any difference between the response of the two telescopes, and will correct for this if it exists. The additional observations made at Lowell should allow us to provide a set of WFPC2 ground standards, and these will be presented separately once the Lowell observations are completed (Holtzman and Watson, in preparation).

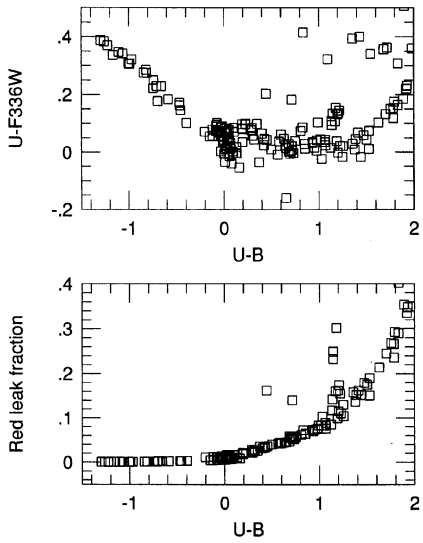

FIG. 3—Synthetic data for F336W showing the difference between F336W magnitudes and U magnitudes (top panel) and the amount of light contributed by red leak (bottom panel) as a function of color. Red leak is defined as contributions from λ>4000 Å.

TABLE 3
Transformations from WFPC2 Ground System to UBVRI[a]

Filter	SMAG	SCOL	T_1	T_2	Z
F336W	U	(U-B)	-0.839±0.028	-0.160±0.020	0.000±0.009
	U	(U-V)	-0.272±0.008	0.048±0.006	0.263±0.003
	U	(U-R)	-0.211±0.005	0.046±0.004	0.307±0.002
	U	(U-I)	-0.175±0.003	0.037±0.002	0.331±0.002
F439W	B	(U-B)	-0.115±0.001	-0.041±0.001	-0.058±0.001
	B	(B-V)	-0.093±0.003	-0.100±0.003	0.000±0.001
	B	(B-R)	-0.056±0.002	-0.044±0.001	0.002±0.001
	B	(B-I)	-0.038±0.001	-0.028±0.001	0.002±0.001
F555W	V	(U-V)	-0.014±0.001	0.005±0.000	-0.011±0.001
	V	(B-V)	-0.050±0.003	0.032±0.002	-0.001±0.001
	V	(V-R)	-0.097±0.005	0.116±0.008	0.001±0.001
	V	(V-I)	-0.045±0.003	0.027±0.002	0.000±0.001
F675W	R	(U-R)	0.038±0.001	-0.005±0.000	0.028±0.001
	R	(B-R)	0.082±0.002	-0.017±0.001	0.003±0.001
	R	(V-R)	0.235±0.006	-0.129±0.009	0.000±0.001
	R	(R-I)	0.215±0.006	-0.081±0.010	0.002±0.001
F702W	R	(U-R)	0.055±0.001	-0.003±0.000	0.039±0.001
	R	(B-R)	0.112±0.003	-0.009±0.001	0.003±0.001
	R	(V-R)	0.309±0.007	-0.055±0.011	0.000±0.001
	R	(R-I)	0.260±0.007	0.076±0.012	0.001±0.001
F814W	I	(U-I)	-0.019±0.001	0.003±0.000	-0.012±0.001
	I	(B-I)	-0.037±0.002	0.007±0.001	0.000±0.001
	I	(V-I)	-0.067±0.003	0.025±0.002	0.000±0.001
	I	(R-I)	-0.127±0.006	0.086±0.010	0.000±0.001

[a] These transformations were derived from stars with color range $-0.3 < B-V < 1.5$ and $-0.3 < V-I < 1.5$. They will most likely be inaccurate for stars outside this range. They may also be inaccurate for objects whose spectra do not match those of the standard stars (see text).

3.3 Transformations to *UBVRI*

The zero-point solutions give the transformations from the WFPC2 ground system to the *UBVRI* system. In addition to the relations of Eq. (3), we determined transformations for several choices of standard color. Table 3 presents the coefficients for transformations of the form:

$$\mathrm{SMAG}=\mathrm{WFPC2}G+T_{1,G}\times\mathrm{SCOL}+T_{2,G}\times\mathrm{SCOL}^2+Z_G \quad (5)$$

where WFPC2G is the WFPC2 ground-system magnitude [M from Eq. (4)], SMAG is the *UBVRI* standard magnitude, SCOL is the standard color in the *UBVRI* system, $T_{1,G}$ and $T_{2,G}$ are the transformation coefficients (for the ground system) and the zero point, Z_G, is zero by definition for the standard colors used in the zero point definition, but may be nonzero for other choices of standard color. Note that we

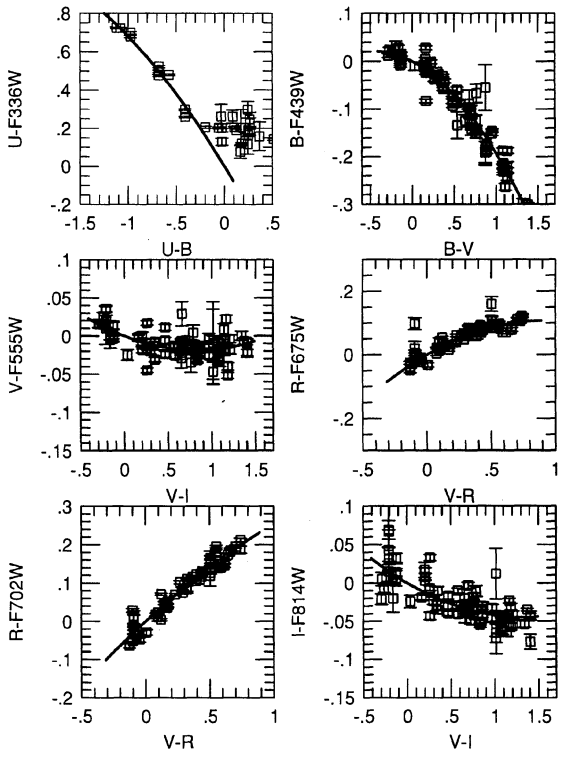

FIG. 4—Observed transformations between the WFPC2 ground system and *UBVRI*. Individual data points are shown as squares with error bars from photon statistics. The lines show the derived transformations.

have used the standard, not the instrumental color, for the color terms; this has several advantages as discussed by Stetson (1992). The observed standard stars were generally in the color range $-0.3<B-V<1.5$ or $-0.3<V-I<1.5$; the transformations cannot be assumed to be correct for stars with colors outside this range.

Figure 4 shows the individual observed data points along with some of the derived transformations for the six different filters; note that the ordinate scales are not the same for all of the filters. Generally, the fits are good, and the scatter is typically 0.015 mag rms (larger for F439W and F336W); the error bars plotted are from photon statistics and do not include contributions from errors in the extinction coefficient and zero-point determinations. The quoted errors for the transformation coefficients were derived from photon statistics, and thus may underestimate the true errors. The primary errors in the transformation coefficients arise from uncertainties in the second-order extinction coefficients. Switching between the second-order coefficients found by fitting and the synthetic second-order coefficients can change the color terms by as much as 0.03, more for F336W. Fortunately, if these transformations are used in conjunction with color terms obtained for the flight-to-ground transformations to get flight-to-*UBVRI* transformations (Sec. 4), then errors arising from the second-order extinction correction will tend to cancel, since most of the standards are observed at airmasses similar to those at which the flight calibration fields were observed.

Additional data on transformations will be presented in Secs. 5 and 6. We have used the observed transformations, as well as additional data, to check the WFPC2 synthetic system, and as shown in Sec. 5, a reasonable agreement can be made between observations and the synthetic system. The synthetic system can then be used to extend the transformations over a wider range of stellar colors.

However, observers should be cautioned about the use of transformations when interpreting data. Because the WFPC2 bandpasses differ significantly from the *UBVRI* bandpasses, one cannot just transform to *UBVRI* and proceed with interpretation. Transformations can be sensitive to details in the underlying stellar spectra. Consequently, they can depend on metallicity and surface gravity, and may not be the same for reddened objects or for integrated spectra of galaxies as for individual stars. Strictly speaking, these transformations are correct only for stars with spectra which match the observed standards. The observed standards are typically white dwarfs for blue colors, main-sequence stars for intermediate colors, and giants for red colors, so the observed transformations do not provide a set of transformations which is uniform in surface gravity. Metallicities are not known for the Landolt standards. Most, but not all, of the stars have low reddenings. In addition, corrections such as reddening and extinction which depend on the actual observed bandpasses must be made in the WFPC2 system and not to transformed magnitudes. Variations in transformations as a function of metallicity, gravity, and reddening are discussed in Sec. 6, and extinction corrections in the WFPC2 system for known reddenings are discussed in Sec. 7.

3.4 Flight Calibration Fields

Observations were also obtained at SSO of the flight calibration fields in ω Cen and NGC 6752. These provide the data by which the ground system can be tied to the on-orbit photometric system.

The flight calibration fields are somewhat crowded in the ground observations, a circumstance which was difficult to avoid in the choice of the fields because of the desire to get a reasonable number of stars with a range in stellar color in a field that could be observed with a single pointing of *HST*/WFPC2 (Harris et al. 1993). Because of the crowding, the ground photometry was done using profile fitting, using the modified DAOPHOT package (Stetson 1987) within the VISTA image processing package.

The on-orbit observations, discussed in Sec. 4, were used to find stars in the calibration fields; the superior resolution of *HST*/WFPC2 allowed many stars which could not be seen from the ground to be identified. A geometric transformation between the flight coordinates and the ground coordinates was determined from observations of several isolated bright stars after the geometric distortion in WFPC2 was removed from the flight positions (H95). Using this, the on-orbit positions were transformed to positions on each of the ground-based frames, and these provided starting guesses for the profile-fitting routine.

Each field was observed in each filter on at least two of the three photometric nights, and observations in F439W, F555W, and F814W were made on all three nights. On each

TABLE 4
Observations of ω Cen and NGC 6752 at SSO

Field	Filter	Date	Exposure times	Frame numbers
ω Cen	F336W	4/20	600,600	6271-72
		4/21	600,600	7182-83
	F439W	4/20	300,300,600	6260-62
		4/21	300,600,600	7179-81
		4/22	300,600	8281-82
	F555W	4/20	60,60,300,300	6267-70
		4/21	60,300	7177-78
		4/22	60,300	8279-80
	F675W	4/20	60,60,300,300	6273-76
		4/22	60,300	8277-78
	F702W	4/21	30,30,100,300,300	7168-72
		4/22	60,300	8275-76
	F814W	4/20	60,60,300,300	6263-66
		4/21	60,30,300	7173-76
		4/22	60,300	8273-74
NGC 6752	F336W	4/20	600	6340
		4/21	600,600	7291-92
	F439W	4/20	300,600	6338-39
		4/21	300,600	7289-90
		4/22	600,300	8362-63
	F555W	4/20	60,300	6336-37
		4/21	60,300	7287-88
		4/22	45,250	8368-69
	F675W	4/20	60,300	6334-35
		4/22	45,250	8366-67
	F702W	4/21	30,60,300,300	7281-84
		4/22	30,300	8364-65
	F814W	4/20	60,300	6332-33
		4/21	60,300	7285-86
		4/22	45,240	8370-71

night, a minimum of two exposures (short and long) was taken through each filter. A log of the observations is presented in Table 4.

For each frame, between two and seven isolated stars (as determined from the on-orbit data) were chosen to define the point-spread function (PSF) for the frame. All stars were then fit simultaneously with all neighbors falling within $\sim 11''$, solving iteratively for the brightness of each star relative to the PSF and the stellar positions. The background sky level was determined from a modal estimate in an annulus of $\sim 16''$–$27''$, the same as used for the aperture photometry of the standard stars. After solving for the brightnesses of all the stars, the fits were used to subtract all but the stars used to make the PSF, and the PSF was reconstructed from the subtracted frame to improve the rejection of faint stars in the PSF. In addition, revised sky values were determined for every star from the subtracted frame. The magnitudes and positions were then solved for again using the revised PSF and sky values. This iteration was repeated one additional time to get the final magnitudes for the stars. Negligible changes are found with additional iterations.

This procedure gave magnitudes of stars on each frame relative to the brightness of the PSF used for the profile fitting. To convert these relative magnitudes to absolute brightnesses, we used the following technique. For each filter, we chose one short exposure frame on each night to be the fiducial frame. For all other observations in that filter on that night, we determined the relative scaling of the brightnesses by computing a weighted mean magnitude difference for all stars with errors less than 0.1 mag. On the fiducial frame, we then determined an "aperture correction" using the separate PSF stars: we subtracted all other stars, visually inspected the subtracted images and manually median filtered regions of poor subtraction, then performed aperture photometry on each of the PSF stars. This aperture photometry was done interactively, as we carefully adjusted the background level for each star to make the aperture growth curves look similar for each star, and we visually marked the magnitude at the aperture diameter of $22\farcs5$ which was used for the standard stars. Generally, the subtractions were excellent so little filtering was needed on the subtracted images, and the sky values generally needed adjustment by only a few tenths of a DN to get good growth curves. We then computed a weighted mean difference between the large aperture magnitudes and the profile-fit magnitudes to determine the final aperture correction for each of the fiducial frames.

Since we determined a separate aperture correction for each night in each filter, we got some estimate of the accuracy of the correction by checking for agreement between the different nights in the total magnitudes. Generally, this agreement was within 1%–2%. Unexpectedly, the agreement between the different nights was better for ω Cen than it was for NGC 6752, despite the fact that the former field is significantly more crowded.

To get final magnitudes and errors, we averaged the profile results for each star for each night using a weighted mean, after application of the mean differences between the frames and the fiducial frame. The errors used for weighting were those returned by the profile-fitting routine. In the averaging, we rejected observations for which the fitting routine required more than 40 iterations to converge, and also rejected observations for which the goodness-of-fit parameter CHI (see Stetson 1987) was larger than 3; these criteria removed only a very few observations. We also computed the error in the mean and the χ^2_ν of the deviations from the mean. We applied the aperture corrections for each night and corrected the mean magnitudes for extinction using Eq. (4); correcting the mean was valid because the fields were taken at low airmass, and multiple observations through a filter never differed by more than 0.01 in airmass. The zero points from Eq. (4) put the magnitudes on the WFPC2 ground system. Finally, we averaged the observations from the multiple nights. In this averaging, we rejected observations with $\chi^2_\nu > 3$ from the averaging on each night; again, this rejected very few points, and most of those that were rejected were in F336W. A weighted average was used, and both the error in the mean and the observed scatter around the mean was computed. For the final error estimate, we chose the larger of these two values.

The measured WFPC2 ground-system magnitudes for the ω Cen and the NGC 6752 stars will be presented in a separate publication along with the WFPC2 magnitudes of the standard stars.

4. THE WFPC2 FLIGHT PHOTOMETRIC SYSTEM

WFPC2 observations were made of one of the flight calibration fields roughly twice per month during the first year of

TABLE 5
WFPC2 Observations of ω Cen and NGC 6752

Field	Date	Observation IDs	Filters
ω Cen	03/11	u2820201-a	F336W,F439W,F555W,F675W,F814W
	03/14	u2820401-a	F336W,F439W,F555W,F675W,F814W
	03/26	u2820601-a	F336W,F439W,F555W,F675W,F814W
	03/29	u2820801-a	F336W,F439W,F555W,F675W,F814W
	05/28	u2820g01-a	F336W,F439W,F555W,F675W,F814W
	06/06	u2820i01-a	F336W,F439W,F555W,F675W,F814W
	06/16	u2820k01-a	F336W,F439W,F555W,F675W,F814W
	07/17	u2g40401-a	F336W,F439W,F555W,F675W,F814W
	07/25	u2g40601-a	F336W,F439W,F555W,F675W,F814W
	08/01	u2g40801-a	F336W,F439W,F555W,F675W,F814W
	08/25	u2g40a01-a	F336W,F439W,F555W,F675W,F814W
	09/03	u2g40c01-a	F336W,F439W,F555W,F675W,F814W
NGC 6752	09/23	u2g40101-a	F336W,F439W,F555W,F675W,F814W
	09/29	u2g40301-a	F336W,F439W,F555W,F675W,F814W
	10/20	u2g40501-a	F336W,F439W,F555W,F675W,F814W
	10/24	u2g40701-a	F336W,F439W,F555W,F675W,F814W
ω Cen	05/28	u2eo0101-6	F300W,F547W,F569W,F606W,F702W,F785LP
	09/22	u2eo0201-6	F300W,F547W,F569W,F606W,F702W,F785LP
ω Cen	01/22	u22t0101-7	F300W,F547W,F569W,F606W,F702W,F785LP
	01/27	u22t5101-7	F300W,F547W,F569W,F606W,F702W,F785LP

WFPC2 operation through the filters F336W, F439W, F555W, F675W, and F814W as part of ongoing photometric monitors. In addition, observations through additional filters, including F702W, were made three times during the first year. A log of the observations made in this time period is presented in Table 5. A field in ω Cen is the primary calibration field and was observed from 1994 January until 1994 September; after September, the spacecraft roll prevented the acquisition of guide stars, so from September until December, a field in NGC 6752 was observed.

Because of the CTE problem we have restricted the analysis of the ω Cen frames to those taken with the CCDs at −88°C (after 1994 April 23) and we have corrected the photometry with the simple prescription discussed in Sec. 2.1. It is important to note that because we are correcting for CTE, our zero points apply to CTE-corrected data. If a CTE correction is not applied to data, resulting photometry could be off by up to ~4% if the zero points we derive are used, depending on the location of the object and the amount of background light in the frame. Similarly our zero points refer to data taken at −88°C; as discussed in Sec. 2.2, the near-IR QE was different by a few percent at −76°C.

The roll in each field changes with time, so slightly different regions of the field are seen at different times. For several observations at different rolls, stars were marked visually, then the positions were transformed to an undistorted coordinate frame (H95). The lists from the different roll angles were merged into a single master list. For each observation, several bright stars are found, their positions are distortion corrected, and the orientation of the frame is derived. This orientation is applied to the master list, and then the inverse distortion correction is applied to the positions. This yields estimates of the stellar positions on each frame, and these estimates are used as input to an iterative centroiding algorithm. In this way, all stars can be found automatically on any observation and can be easily labelled with consistent identification numbers.

From the master list of stars which contains 1248 (221) stars in ω Cen (NGC 6752), we chose a subset to be used as standard stars. To qualify as a standard star, a star had to have no other stars within 3″ and had to have greater than ~100 DN in the exposures which were used to make the master list. This criterion yielded 42 (33) standards in ω Cen (NGC 6752).

TABLE 6
Transformations from WFPC2 Flight System to Ground System[a]

Filter	Standard Color	T_1	Z
F336W	(F336W-F439W)	-0.003±0.009	18.505±0.003
	(F336W-F555W)	0.026±0.006	18.494±0.004
	(F336W-F675W)	0.027±0.005	18.483±0.005
	(F336W-F814W)	0.025±0.004	18.477±0.005
F439W	(F336W-F439W)	0.043±0.007	20.139±0.003
	(F439W-F555W)	0.092±0.006	20.069±0.004
	(F439W-F675W)	0.058±0.004	20.065±0.005
	(F439W-F814W)	0.047±0.003	20.063±0.005
F555W	(F336W-F555W)	0.001±0.003	21.718±0.002
	(F439W-F555W)	-0.011±0.005	21.727±0.004
	(F555W-F675W)	-0.018±0.009	21.728±0.004
	(F555W-F814W)	-0.008±0.006	21.725±0.005
F675W	(F336W-F675W)	0.012±0.003	21.232±0.003
	(F439W-F675W)	0.013±0.004	21.231±0.005
	(F555W-F675W)	0.025±0.011	21.234±0.006
	(F675W-F814W)	0.088±0.018	21.220±0.006
F814W	(F336W-F814W)	0.008±0.003	20.831±0.004
	(F439W-F814W)	0.006±0.004	20.834±0.006
	(F555W-F814W)	0.005±0.008	20.839±0.006
	(F675W-F814W)	0.011±0.019	20.840±0.006

[a]These coefficients should be used with the transformation given by Eq. (6). As discussed in the text, the quoted zero points refer to 0.″5 radius aperture measurements after correction for CTE effects.

All observations were made with the gain=14 channel (electronics bay 3). All the data were reduced using the methods discussed by H95. The data were flat-fielded with the flats which were installed in the STScI database in 1994 March. During each run, two observations of identical exposure time were made through each filter. These two observations were compared to identify cosmic rays. Any pixel which was found to deviate more than expected from the noise characteristics of the detectors was flagged as a cosmic ray. Aperture photometry was then performed on all of the stars in each of the two frames separately, using a 0.″5 radius aperture. If a flagged pixel was found in the aperture, the measurement was discarded. No aperture corrections were applied, so all derived zero points refer to measurements in a 0.″5 radius aperture, as discussed in Sec. 2.5.

These data were used to derive transformations between the WFPC2 flight system and the ground system. It was expected that color terms between these systems should be small, because the systems differ only by an additional five reflections in the flight system and the use of a slightly different set of filters (with the same specifications). The extra reflections are expected to only introduce tiny color terms; however, some of the filters, even though they are flight spares, differ in bandpass enough to introduce small color terms (see Fig. 2). The ground-system response also contains the atmospheric transmission, but we have attempted to remove this through the use of extinction coefficients; some differences may still exist in the near-UV because of uncertainties in the extinction corrections.

The derived transformations are presented in Table 6. These give relations of the form:

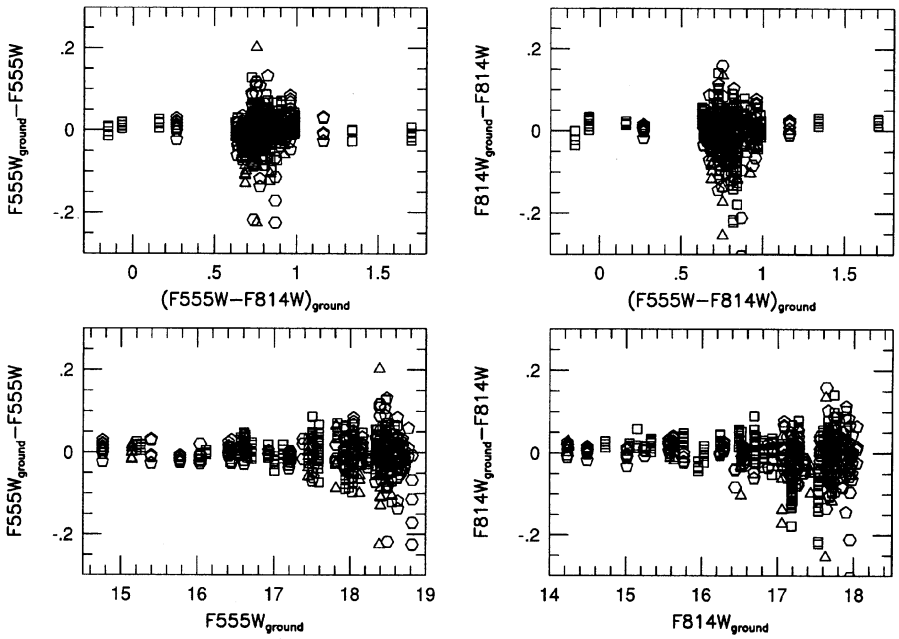

FIG. 5—Residuals from the flight-to-ground WFPC2 transformations for F555W (left) and F814W (right) as a function of color (top) and magnitude (bottom). Different point types represent the four different chips (PC1, triangles; WF2, squares; WF3, pentagons; WF4, hexagons).

$$\text{WFPC2}G = -2.5 \times \log \text{DN s}^{-1} + T_{1,FG} \times \text{SCOL} + Z_{FG} + 2.5 \log GR_i \quad (6)$$

where WFPC2G is the WFPC2 ground-system magnitude, SCOL is the standard color in the WFPC2 ground system, $T_{1,FG}$ gives the linear color term between the flight and ground systems, Z_{FG} is the zero point, and GR$_i$ is the gain ratio defined in Sec. 2.4 (which is unity for observations made with gain=14). Note that SCOL is defined to be the color in the ground system; this can be derived algebraically if observations are made in more than one flight filter. Because the two systems have very similar response, only a linear color term was derived. The uncertainties in the gain ratio discussed in Sec. 2.4 propagate directly into uncertainties in the bay 4 photometric zero points.

Most of the stars in the flight calibration fields have colors typical of globular-cluster giants. There are just a few blue stars, which are horizontal-branch stars in the clusters, and very red stars, which are probably foreground objects. The limited number of stars at the color extremes makes the derived color terms more uncertain. In practice, the derived values can be sensitive to the weighting used for the fits because of the small number of stars which contain color term information. For a first pass, we weighted the fits by the observed errors from the flight measurements with the errors for the ground measurements added in quadrature. With this weighting we typically got $\chi^2_\nu \sim 2$ for the fit. The few brightest stars had errors of <0.01 mag. We rederived fits imposing a minimum error for each point and chose the minimum error to be the value which gave a $\chi^2_\nu \sim 1$. This resulted in using a minimum error of 0.03 mag for the weighting. We feel this is justified because the fit should not be dominated by observations of just two or three stars, and small systematic errors are most likely present which are not included in the original error estimates. The revised errors for the magnitudes were used to derive the uncertainties on the transformation coefficients in Table 6.

Table 6 shows that the color terms in the flight-to-ground transformations are typically small. The largest color terms are for the F439W and the F675W filters. Some color terms are expected because the ground filters differ slightly from the flight filters (Fig. 2). For F439W, the observed color term in F439W is 0.09, while the predicted value is 0.055; in F675W, the observed value is 0.023, while the predicted value is very nearly zero. The typical formal errors on the color terms are 0.005–0.010. Some of the difference between the observed and predicted values may arise from errors in the second-order extinction from the ground. As mentioned previously, however, these should cancel to first order when the flight-to-ground transformations are used in conjunction with the ground-to-*UBVRI* transformations. However, observers are cautioned that color terms might be in error, especially for F439W and F675W.

Some sample transformation residuals for F555W and F814W are shown in Fig. 5. This figure plots the magnitude residuals (ground-flight) against both stellar color and stellar magnitude. Different symbols represent the different chips. The limited number of stars of extreme color is readily apparent, and, by chance, almost all of these stars happen to lie in WF2. Consequently, there is no real information about possible color term variations from chip-to-chip, although none are expected because the QE curves of the chips were measured to be very similar and because the filter passbands were measured to be very constant across the entire filter (a single filter is used for all of the chips). No trends with magnitude are readily visible, suggesting that CTE effect has

TABLE 7
Transformations from WFPC2 Flight System to UBVRI[a]

Filter	SMAG	SCOL	T_1	T_2	Z
F336W	U	(U-B)	-0.844±0.030	-0.160±0.020	18.505±0.010
	U	(U-V)	-0.240±0.010	0.048±0.006	18.764±0.005
	U	(U-R)	-0.172±0.007	0.041±0.004	18.797±0.006
	U	(U-I)	-0.149±0.005	0.038±0.002	18.817±0.006
F439W	B	(U-B)	-0.103±0.009	-0.046±0.002	20.057±0.005
	B	(B-V)	0.003±0.007	-0.088±0.003	20.070±0.004
	B	(B-R)	0.019±0.005	-0.049±0.001	20.064±0.005
	B	(B-I)	0.005±0.003	-0.023±0.001	20.067±0.005
F555W	V	(U-V)	-0.014±0.004	0.005±0.000	21.706±0.003
	V	(B-V)	-0.060±0.006	0.033±0.002	21.725±0.004
	V	(V-R)	-0.121±0.011	0.120±0.008	21.730±0.004
	V	(V-I)	-0.052±0.007	0.027±0.002	21.725±0.005
F675W	R	(U-R)	0.039±0.004	-0.007±0.001	21.254±0.003
	R	(B-R)	0.092±0.005	-0.017±0.001	21.235±0.005
	R	(V-R)	0.253±0.013	-0.125±0.009	21.234±0.006
	R	(R-I)	0.273±0.020	-0.066±0.011	21.225±0.006
F814W	I	(U-I)	-0.018±0.004	0.002±0.001	20.815±0.004
	I	(B-I)	-0.031±0.004	0.007±0.001	20.835±0.006
	I	(V-I)	-0.062±0.009	0.025±0.002	20.839±0.006
	I	(R-I)	-0.112±0.021	0.084±0.011	20.839±0.006

[a]These coefficients should be used with the transformation given by Eq. (8). As discussed in the text, the quoted zero points refer to 0".5 radius aperture measurements after correction for CTE effects.

been well-corrected and that there are no linearity problems, although these measurements do not extend to very faint objects. We have made separate solutions for each chip individually and find that zero points for each chip agree with the mean value to within 2% after correction for the variation in pixel area between the cameras (see Sec. 2.3.1), indicating that the that field fields are reasonably accurate.

The WFPC2 flight photometric system is defined by the on-orbit response, with zero points set such that flight magnitudes match ground magnitudes for stars of zero color. This also makes flight magnitudes match *UBVRI* for these stars. Consequently, WFPC2 flight magnitudes are defined to be:

$$\mathrm{WFPC2} = -2.5 \times \log(\mathrm{DN\ s^{-1}}) + Z_{FG} + 2.5 \times \log GR_i, \quad (7)$$

where the zero points are those given in Table 6.

The flight-to-ground transformations have been combined with the ground-to-*UBVRI* transformations in Table 3 to determine flight-to-*UBVRI* transformations, which are presented in Table 7. There are several routes to these transformations depending on the standard colors used in each transformation; the values in Table 7 for each standard color were derived by going through the ground filters analogous to the standard colors. The coefficients in Table 7 are used for transformations of the form:

$$\mathrm{SMAG} = -2.5 \times \log(\mathrm{DN\ s^{-1}}) + T_{1,FS} \times \mathrm{SCOL} + T_{2,FS} \times \mathrm{SCOL}^2 + Z_{FS} + 2.5\ \log GR_i, \quad (8)$$

where SMAG and SCOL are the standard magnitude and color, $T_{1,FS}$ and $T_{2,FS}$ are the flight-to-*UBVRI* transformation coefficients, Z_{FS} is the zero point, and GR_i is the gain ratio. SCOL is defined as the *UBVRI* color and consequently must be derived iteratively using WFPC2 observations in two colors unless the color is known or can be estimated *a priori*. Some reasons for using the standard color have been discussed by Stetson (1992); if one wishes to avoid iteration (we cannot quite imagine why), the WFPC2 colors after application of zero points could be substituted for the standard colors with some systematic errors that would increase as the stellar color departed from zero and would be worse for bandpasses which are not close to the *UBVRI* bandpasses. The same caveats apply to the use of these transformations as were discussed for the ground-to-*UBVRI* transformations: there may be metallicity, gravity, and reddening dependences and the transformations may not be accurate for objects of extreme color. The accuracy of these transformations is estimated to be $\lesssim$2% judging from the scatter in the ground-to-*UBVRI* transformations and from uncertainties in the derived on-orbit zero points.

The QE of the WFPC2 CCDs changed slightly in the near IR when the CCD temperatures were changed on 1994 April 23. Because only data from −88 °C was used in determining transformations, the photometric zero points presented here apply to −88 °C. For −76 °C data, we measured that the QE through F814W was higher by ~5% (H95). Consequently, observers should add ~5% to the near-IR zero points if they are being applied to data taken at −76 °C. At F555W, we believe there was little change in the QE with the change in temperature; at intermediate wavelengths between 6000 and 8000 Å, there was probably a change of a few percent.

Since the photometric zero points have been determined for counts with a 0.5 radius aperture, they are not directly applicable for surface photometry. To do surface photometry, one generally wants zero points which refer to total light from an object. Consequently, to apply the zero points to surface photometry, they should be corrected to give the light collected in a large aperture, as discussed in Sec. 2.5. The correction is roughly 10% in the sense that the zero points should be increased by about 0.1 mag.

4.1 Comparison with *UBVRI* Photometry

Observations of both spectrophotometric standards and ω Cen can be used to check the derived transformations because *UBVRI* photometry exists for the spectrophotometric standards (Landolt, private communication) and *BVRI* photometry exists for ω Cen (Walker 1994). Since the spectra of these stars may differ from those used to derive the transformations, the resulting transformed magnitudes may not agree perfectly with the observed *UBVRI* magnitudes, but they should be close. The spectrophotometric standards have excellent *UBVRI* measurements, with errors <0.01 mag, but the ω Cen measurements are of lower quality, with errors of up to several percent for the fainter stars.

Figure 6 shows the difference between the transformed *UBVRI* magnitudes and the standard magnitudes as a function of stellar color. Different symbol types are for the different stars; filled symbols show −88 °C data, while open symbols are used for the −76 °C data. Generally, the transformations appear to give reasonable magnitudes. Some errors might be expected from the application of the crude correction for CTE, especially for the data taken at −76 °C. The agreement between the transformed and standard magnitudes for the spectrophotometric stars is within 2% in all filters except for F336W and F814W for −88 °C data. The

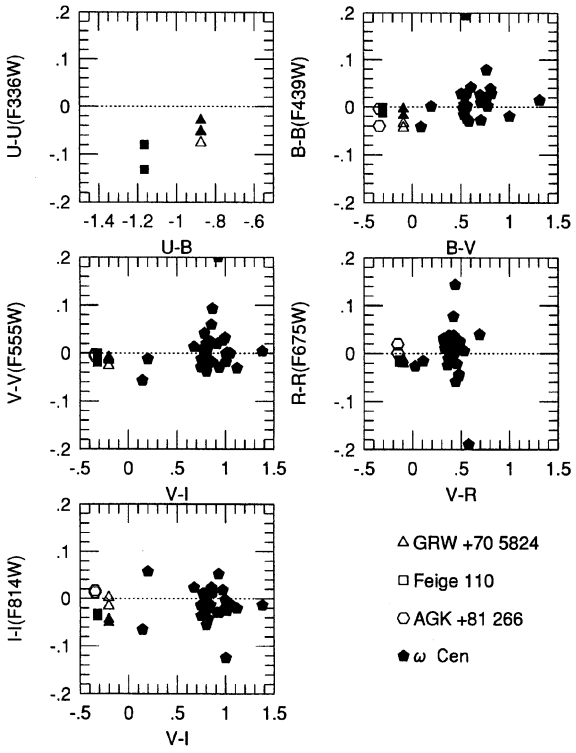

FIG. 6—Comparison of WFPC2 observations transformed to *UBVRI* with standard *UBVRI* magnitudes for several spectrophotometric standards and for stars in ω Cen. Different point types represent the different fields; filled points are −88 °C data and open points are −76 °C data.

F814W results may be off because the true transformation between F814W and *I* for very blue stars is not well represented by the quadratic fit used here (see Fig. 3, and later, Fig. 9). The discrepant results for Feige 110 in F336W are not well understood. The ω Cen results show larger scatter, but this is probably consistent with errors in the ground measurements.

Since perfect matches cannot be expected because of the differences in spectral type between these stars and the calibration standards, it is difficult to use these comparisons to assess true errors in the WFPC2-to-*UBVRI* transformations; however, these results suggest that such errors are $\lesssim 2\%$.

4.2 Additional Observations of Flight Calibration Fields

Observations have also been made in ω Cen through several additional filters, but only twice to date at −88 °C. These data are not currently useful for deriving accurate flight-to-*UBVRI* transformations because we did not obtain ground-based WFPC2 photometry in these filters (except for F702W). Transformations could be directly derived using the *BVRI* photometry in ω Cen from Walker (1994); however, these transformations will suffer from uncertainties arising from the limited color range of the stars. We have chosen to use synthetic results to calibrate these filters, since we found good agreement between the synthetic and observed transformations for the primary filters (Sec. 5).

The ω Cen observations in these filters might also be used to check the synthetic calibration by comparing with stellar isochrone data.

5. THE WFPC2 SYNTHETIC SYSTEM

5.1 WFPC2 System Response Curves

The WFPC2 synthetic system consists of a set of response curves which give the transmission/reflectance/response of all of the components which determine the response of the instrument. Estimates were made of these curves before launch for the following components: optical telescope assembly (OTA), instrument reflections, filter transmissions, and CCD+MgF window response. These formed our first estimate of the WFPC2 synthetic system.

Given response curves, count rates can be predicted for stars for which we have spectrophotometry. The spectra give photon rates as function of wavelength, which are multiplied by the response curves and are integrated over wavelength. Absolute count rates are estimated using the gain of the CCDs and knowledge of the telescope area and obscurations from the telescope primary mirror pads, the telescope secondary and spiders, and the WFPC2 optics. We originally attempted to make our best predictions for count rates at the centers of each of the CCDs; the vignetting by the instrument optics depend on field location. However, the observed count rates are modified when flat fields are applied to give uniform results across the field. Since we have found that we need to make some adjustments to the prelaunch predictions for responses, in practice we have just made these adjustments to match the observed count rates after flat fielding. Thus our synthetic system is tied to the flat-field normalization, but independent of the exact value of the gain or the field location. We have defined the synthetic response curves to give correct values using the current flat fields with an assumed gain of 14 e^-/DN and for total counts within a 0.5 radius aperture. This is consistent with our definition of the observed zero points presented in previous sections.

The OTA response curves were taken from Perkin-Elmer measurements of the *HST* primary and secondary before launch. The final OTA curve was the product of the reflectances of both mirrors plus an additional ~10% wavelength-independent loss to account for dust on the mirrors. The WFPC2 response curve was originally derived from taking a mirror reflectance curve from one of the WFPC2 witness mirrors and raising it to the fifth power (because there are five reflections inside the instrument). However, this curve did a poor job of predicting count rates, especially in the UV, where it overestimated the instrument throughput. Instead of using this, we have taken the OTA curve, removed the dust component, and raised it to the 5/2 power to make a WFPC2 throughput curve. This is justified because both the OTA and the WFPC2 mirrors are MgF-coated aluminum, and because it appears to match the observed rates better. The filter transmissions were measured from the flight filters at JPL before launch. The CCD+MgF response curves were measured for each of the flight chips before launch; the response for all four chips has a similar shape, and we use the average of the

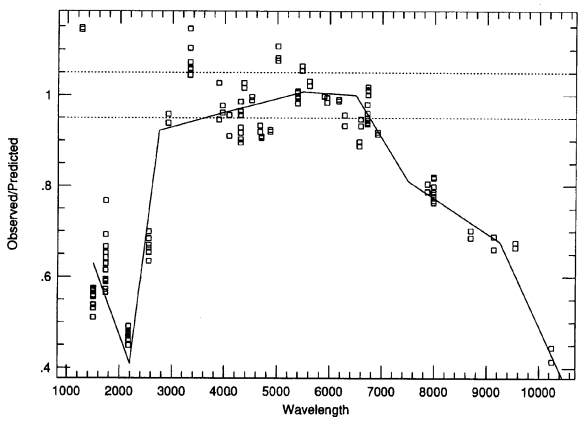

FIG. 7—Ratio of observed-to-predicted count rates using our original estimates of response curves. Solid line shows the derived correction curve for the response.

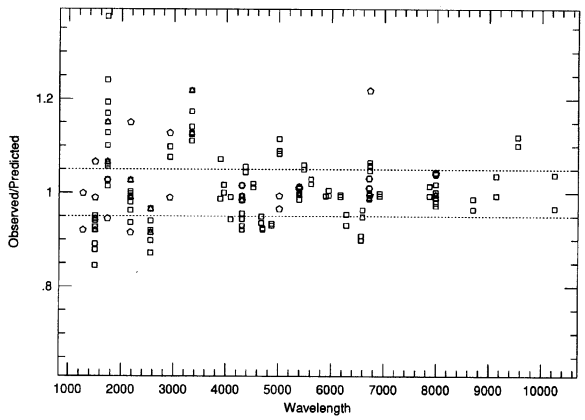

FIG. 8—Ratio of observed to predicted count rates after application of the correction curve for the response. No filter scalings have been applied to these data.

four flight chips. Any absolute differences in QE between the chips is removed by flat fielding, so an average curve is appropriate.

Modifications to response curves were made by comparing the prelaunch predictions to the observed count rates for the four spectrophotometric standards. A grid of wavelength points was chosen and a linear least-squares routine was used to determine the response change needed at each of these points to match the observations. Linear interpolation was used to get the response change between the chosen wavelength points. After some experimentation to get a fairly smooth correction curve, we settled on using nine wavelength points at which we solved for response corrections.

Several complications arose with this procedure. First, although the stars are spectrophotometric standards, there are still uncertainties in the spectrophotometry, which is combined from several sources including observations by Oke (1990) and by *IUE* (Bohlin et al. 1990). Oke (1990) and Colina and Bohlin (1994) discuss errors in normalization of the spectra. The latter paper demonstrates, by comparison with photometry by Landolt (unpublished), that the spectrophotometry of Oke (1990) can be systematically off by several percent for the standard stars. We have used the suggested offsets from Colina and Bohlin for each of our flux standards to scale the spectrophotometry. This resulted in a better agreement between stars than when the raw numbers were used.

Another problem is that the transition from optical data to *IUE* data is not always smooth. Absolute flux calibration at 3200 Å is difficult both for *IUE* and ground spectra. Any systematic errors in the spectrophotometry with wavelength will translate directly into errors in the derived response curves.

The observed count rates relative to synthetic rates using our first estimate (before corrections) of response curves are shown in Fig. 7. The observed count rates have been corrected for CTE effects and for contamination using the prescriptions given in Sec. 2. It is apparent that there are systematic errors as a function of wavelength. In addition, it appears that the filter transmissions curves may have individual normalization errors at the several (5–10+)% level. This is inferred because there is significant scatter around a smooth variation with wavelength, and we believe that the throughput curves should vary smoothly. The technique used for measuring the filter curves probably allows for some errors in normalization (Trauger, private communication), so this is not totally surprising. We have found that the narrow-band filters appear to deviate from a smooth response change more than the broad-band filters, suggesting larger normalization errors for the narrow-band filters. Consequently we derived a correction curve based only on broad-band filter data. This curve is shown as the solid line in Fig. 7. The resulting ratios after this correction curve is applied are shown in Fig. 8. Now, most broad-band filter observations are matched to within five percent; narrow-band observations have more scatter.

Unfortunately, when we only use the broad-band filters, there is some difference in the derived response curve depending on the choice of the wavelength grid on which response changes are derived. We have attempted to make the derived response curve smooth; however, in some wavelength regions, there could certainly be several percent error in the derived curve. In particular, the correction curve is least well constrained where there are only a few filters. This is true in the UV and in the near IR. The reddest correction point is determined entirely from the F1042M filter, so consequently any errors in the filter curve for this filter will result in errors in the system throughput at the reddest points.

In the UV, there is significant scatter in the observed points which comes in part from errors in flat fielding discussed in Sec. 2.3. Also, no monotonic curve was able to accurately match all of the observations in the UV. We chose to allow the derived curve with a dip around 2000 Å because it is plausible that the lower response in the UV is caused by some contaminant in the system, and many contaminants have an absorption peak around 2000 Å. It is very possible that there are differences in contamination in the different chips, and if so, there would be both absolute sensitivity differences as well as different shaped response functions for the different channels. Consequently, our derived UV re-

TABLE 8
Filter Scalings and Efficiencies[a]

Filter	Scale Factor	$\int qtd\lambda/\lambda$	$\bar{\lambda}$	$d\lambda$	q_{max}	σ	$d\lambda/d\alpha$
F122M[b]	1.38	0.00011	1420.	395.	0.00115	0.11802	19.78
F160W	0.88	0.00021	1491.	446.	0.00064	0.12697	24.04
F170W	1.16	0.00057	1747.	548.	0.00168	0.13316	30.98
F185W[c]	1.00	0.00034	1953.	340.	0.00176	0.07403	10.70
F218W	0.96	0.00057	2189.	396.	0.00273	0.07675	12.90
F255W	0.91	0.00078	2587.	394.	0.00450	0.06473	10.84
F300W	1.08	0.00519	2942.	733.	0.01847	0.10580	32.93
F336W	1.14	0.00399	3341.	382.	0.02792	0.04857	7.88
F343N[c]	1.00	0.00005	3433.	24.	0.00674	0.00291	0.03
F375N[c]	1.00	0.00006	3737.	24.	0.00771	0.00277	0.03
F380W	1.01	0.00691	3966.	672.	0.03368	0.07198	20.55
F390N	1.03	0.00029	3889.	45.	0.01875	0.00495	0.10
F410M	0.96	0.00163	4090.	147.	0.03599	0.01525	0.95
F437N	1.05	0.00019	4369.	25.	0.02660	0.00245	0.03
F439W	0.94	0.00500	4300.	473.	0.03412	0.04674	9.39
F450W	1.01	0.01499	4519.	957.	0.07903	0.08988	36.51
F467M	0.94	0.00216	4669.	167.	0.04810	0.01518	1.08
F469N	0.92	0.00023	4694.	25.	0.03256	0.00226	0.02
F487N	0.93	0.00029	4865.	26.	0.04212	0.00226	0.02
F502N	1.10	0.00037	5013.	27.	0.05206	0.00228	0.03
F547M	1.05	0.01223	5476.	483.	0.10465	0.03747	7.69
F555W	1.00	0.02724	5397.	1226.	0.10205	0.09645	50.21
F569W	1.02	0.02136	5614.	965.	0.10474	0.07303	29.94
F588N	0.99	0.00133	5893.	49.	0.11996	0.00353	0.07
F606W	1.00	0.04182	5934.	1498.	0.13296	0.10719	68.18
F622W	0.99	0.02641	6162.	917.	0.12927	0.06316	24.59
F631N	0.96	0.00078	6306.	31.	0.11617	0.00208	0.03
F656N	0.90	0.00045	6563.	21.	0.10322	0.00139	0.01
F658N	0.96	0.00062	6591.	28.	0.10486	0.00184	0.02
F673N	1.06	0.00103	6732.	47.	0.11007	0.00298	0.06
F675W	0.99	0.02163	6697.	866.	0.12570	0.05494	20.22
F702W	1.00	0.03172	6862.	1378.	0.13154	0.08525	49.87
F785LP	0.98	0.00777	8621.	1327.	0.04425	0.06535	36.82
F791W	1.00	0.01561	7828.	1216.	0.09029	0.06594	34.04
F814W	1.00	0.01772	7924.	1500.	0.09845	0.08039	51.21
F850LP	1.01	0.00396	9070.	988.	0.03484	0.04624	19.39
F953N	1.06	0.00012	9545	52	0.01650	0.00234	0.05
F1042M[c]	1.00	0.00012	10190.	403.	0.00349	0.01680	2.88

[a]The definition of quantities in this table can be found in the WFPC2 Instrument Handbook.
[b]The response for F122M is very poorly determined from the current data. In addition, F122M may have significant red leak. Quantities for this filter are very uncertain.
[c]The filter scalings for these filters are not known accurately because no observations were made or because the system response is poorly constrained at these wavelengths.

sponse curve has significant uncertainties. For the furthest UV filter, F122M, very little throughput data were available and the filter has a large red leak, so results are even more uncertain.

We have taken the deviations of the observations from the modified predictions to scale each filter individually, preserving the shape of the filter bandpass, but scaling the throughputs so that the predicted count rates match the observed ones. Table 8 presents the scaling factors applied to each of the filters. The table also presents the dimensionless efficiencies ($\int qtd\lambda/\lambda$), the mean wavelengths ($\bar{\lambda}$), and various other quantities about the bandpasses. Definitions of these quantities are presented in the WFPC2 Instrument Handbook.

It is possible that the derived response curves could still be off by a few percent, probably more in the UV and the near IR. As long as the modified filter curves are used with the modified response curves, correct count rates will be derived for objects which have spectra similar to the spectrophotometric standards (hot stars). For different spectra, the predicted count rates will be in error if the derived response curves and filter normalizations are off, but, at least in the visible part of the spectrum, we expect that such errors will be small (probably less than 1% for any reasonable spectrum), as significant errors in the slope of the response across any filter are unlikely. The response in the UV is more uncertain.

No data were taken of the spectrophotometric standards for the filters F185W, F343N, F375N, or the quad or ramp filters. Consequently, the only throughput information we have for these filters comes from prelaunch estimates, and synthetic photometry through these filters is more uncertain.

The response curves were derived mostly from observations of spectrophotometric standards taken with the current CCD temperature of −88 °C. As discussed above, the QE in the near IR was higher by ~5% when the CCDs were at −76 °C, so the response curves would need to be increased in the near IR if one wanted results at −76 °C.

All of the modified response curves are available from STScI. There are separate files for the OTA response, the corrected instrument response, the filter responses, and the CCD response. We have constructed a single system (*HST* +WFPC2+CCD) response file which has the correct total obscuration, and this file can be used in conjunction with individual filter curves to predict count rates. To predict count rates using the system response curve, use a collecting area of πR^2, with $R=120$ cm, and a gain of $14e^-$/DN for bay 3 observations. To get count rates for bay 4 observations, multiply by the gain ratio discussed in Sec. 2.4. The response curves are appropriate to match integrated brightnesses using a 0.″5 radius aperture.

5.2 WFPC2 Synthetic Zero Points

To calculate synthetic magnitudes, we had to choose a zero-point definition. We have chosen the synthetic system zero points such that the WFPC2 synthetic magnitudes for Vega match the observed *UBVRI* magnitudes in the *UBVRI* filter nearest in wavelength to the WFPC2 filter. For observed Vega magnitudes we have adopted the values 0.02, 0.02, 0.03, 0.039, and 0.035 for U, B, V, R, and I (see references in Worthey 1994). For UV filters we have just set the magnitude of Vega to 0; see Sec. 5.4 for more discussion on UV calibration. A model spectrum for Vega (Kurucz 1992), normalized to the observed Vega flux (Hayes 1985), was used to derive the Vega synthetic magnitudes; the model spectrum for Vega matches the observed spectrum very closely (see, e.g., Worthey 1994) and samples the hydrogen lines more accurately than available observed spectra. As noted previously, this definition for the synthetic zero points does not quite match the definition of the observed zero points from Secs. 3 and 4 because the observed zero points match WFPC2 and *UBVRI* magnitudes for observed standard stars of color zero, which have higher surface gravity than Vega.

The synthetic zero points for all filters are determined by calculating the count rate for Vega through the different passbands. These zero points are presented in Table 9. The synthetic zero points can be used in Eq. (7) to get magnitudes in the WFPC2 synthetic system. Also shown in Table 9 are the

TABLE 9
Synthetic Zero Points[a]

Filter	Z_{syn}	Z_{obs}	$F_\lambda(m=0,\bar{\lambda})$	Z_{STMAG}
F336W	18.539	18.505	3.269E-09	18.656
F439W	20.045	20.070	7.056E-09	19.362
F555W	21.723	21.725	3.838E-09	21.693
F675W	21.237	21.234	2.016E-09	21.894
F814W	20.844	20.839	1.189E-09	22.055
F122M	12.843		4.953E-09	13.306
F160W	13.901		5.572E-09	13.645
F170W	15.466		5.506E-09	15.124
F185W	15.082		5.276E-09	14.738
F218W	15.717		4.478E-09	15.530
F255W	16.211		3.631E-09	16.231
F300W	18.575		3.565E-09	18.621
F380W	20.119		5.938E-09	19.541
F410M	18.805		6.127E-09	18.020
F450W	21.173		6.395E-09	20.672
F467M	19.160		5.868E-09	18.645
F547M	20.839		3.670E-09	20.831
F569W	21.419		3.414E-09	21.501
F606W	22.084		2.893E-09	22.368
F622W	21.543		2.571E-09	21.932
F702W	21.628		1.872E-09	22.368
F785LP	19.877		9.857E-10	21.351
F791W	20.707		1.236E-09	21.883
F850LP	19.140		9.059E-10	20.737
F1042M	15.367		6.230E-10	17.324
F343N				14.085
F375N				14.283
F390N				16.013
F437N				15.877
F469N				16.228
F487N				16.558
F502N				16.852
F588N				18.578
F631N				18.142
F656N				17.631
F658N				18.005
F673N				18.598
F953N				17.026

[a]As discussed in the text, the quoted zero points refer to 0.″5 radius aperture measurements after correction for CTE effects.

observed zero points for the five filters in which we made ground observations. The agreement is excellent for F555W, F675W, and F814W. For F336W and F439W, there is a difference between the observed and synthetic zero points, but this was expected because of surface-gravity effects; in fact, the differences are close to those expected from synthetic photometry of stars with different surface gravities. The physical zero points of the system in ergs cm^2 s^{-1} Å, $F_\lambda(m=0,\bar{\lambda})$, are also presented. These give the monochromatic flux at the effective wavelength of the filter ($\bar{\lambda}$ in Table 8) for an object with a spectrum the shape of Vega and $m=0$. No zero points or fluxes relative to Vega are presented for the narrow-band filters; see Sec. 9.5.

We also give the zero points for the the STScI magnitude system (STMAG), which relates physical flux to magnitudes for a constant F_λ spectrum: STMAG$=-2.5\times\log F_\lambda - 21.1$. Consequently, in the STMAG system, an object with a flat F_λ, spectrum and $m=0$ has a monochromatic flux of $F_\lambda=3.63\times10^{-9}$ ergs cm^2 s^{-1} Å. The zero points in Table 9 can be used to put observed WFPC2 count rates onto the STMAG system using STMAG$=-2.5\times$DN s^{-1} $+Z_{\rm STMAG}+2.5\times\log {\rm GR}_i$. Using STMAG units gives the conversion from counts to monochromatic flux for a flat spectrum object. Note that STMAG system magnitudes will differ significantly from the WFPC2 system magnitudes which are defined relative to Vega.

The zero points given in Table 9 are probably accurate to within 2%, judging from the degree to which synthetic predictions match observed count rates, the agreement with observed zero points, and uncertainties in photometry from CTE and flat fielding.

As with the observed zero points, the synthetic zero points are derived for point sources as measured with a 0.″5 radius aperture. For surface photometry, these zero points must be adjusted as discussed in Sec. 2.5.

5.3 WFPC2 Synthetic Transformations

The synthetic curves were derived from observations of hot spectrophotometric standards. As a check on the curves, we can compute synthetic transformations between the WFPC2 system and the *UBVRI* system using the BPGS stellar atlas, and compare them with the observed transformations derived from the flight calibration fields and the observations of the standards from the ground. This check is not conclusive because we must assume that we have an accurate synthetic representation of the *UBVRI* system, and also that the BPGS library is accurate.

For the synthetic *UBVRI* photometry, we first used the *UBVRI* response curves from Landolt (1992a), which are those of his CTIO system, and also applied transformations (Landolt 1992a) to bring the magnitudes onto the standard Landolt system (Landolt 1973, 1983). However, we got poor agreement with the observed WFPC2 transformations using these results. We compared synthetic *UBVRI* photometry for spectrophotometric standards with Landolt *UBVRI* measurements, and found significant color terms, strongly suggesting that the *UBVRI* response curves are in error. We then used the Landolt response curves from KPNO along with KPNO transformations (Landolt, private communication) and got significantly better results for both the WFPC2 comparison using the BPGS atlas and for the *UBVRI* comparison on spectrophotometric standards, except for *U*. In the *U* band, there is a systematic error in the synthetic *U* magnitudes compared with the observed *U* magnitudes as a function of color for spectrophotometric standards which have Landolt observations. We also tried using the *UBVRI* curves of Bessell (1990), who provides an excellent discussion on variations of *UBVRI* systems and best estimates of response curves to match these systems. Bessell, however, derives curves to match the Johnson–Cousins *UBVRI* system, which he finds to differ very slightly from the Landolt *UBVRI* system, even though they are supposed to be the same. Since all of our standards stars were standards measured by Landolt, we have chosen to use the Landolt (KPNO) curves for synthetic *UBVRI* photometry, and in fact, these provide the best matches to our observed transformations. None of the choices of filter curves for the *U* band gave good results for the spectrophotometric stars, so we believe that the synthetic *U* results are probably incorrect.

The synthetic transformation data for the primary photometric filters are presented in Fig. 9. The crosses are the

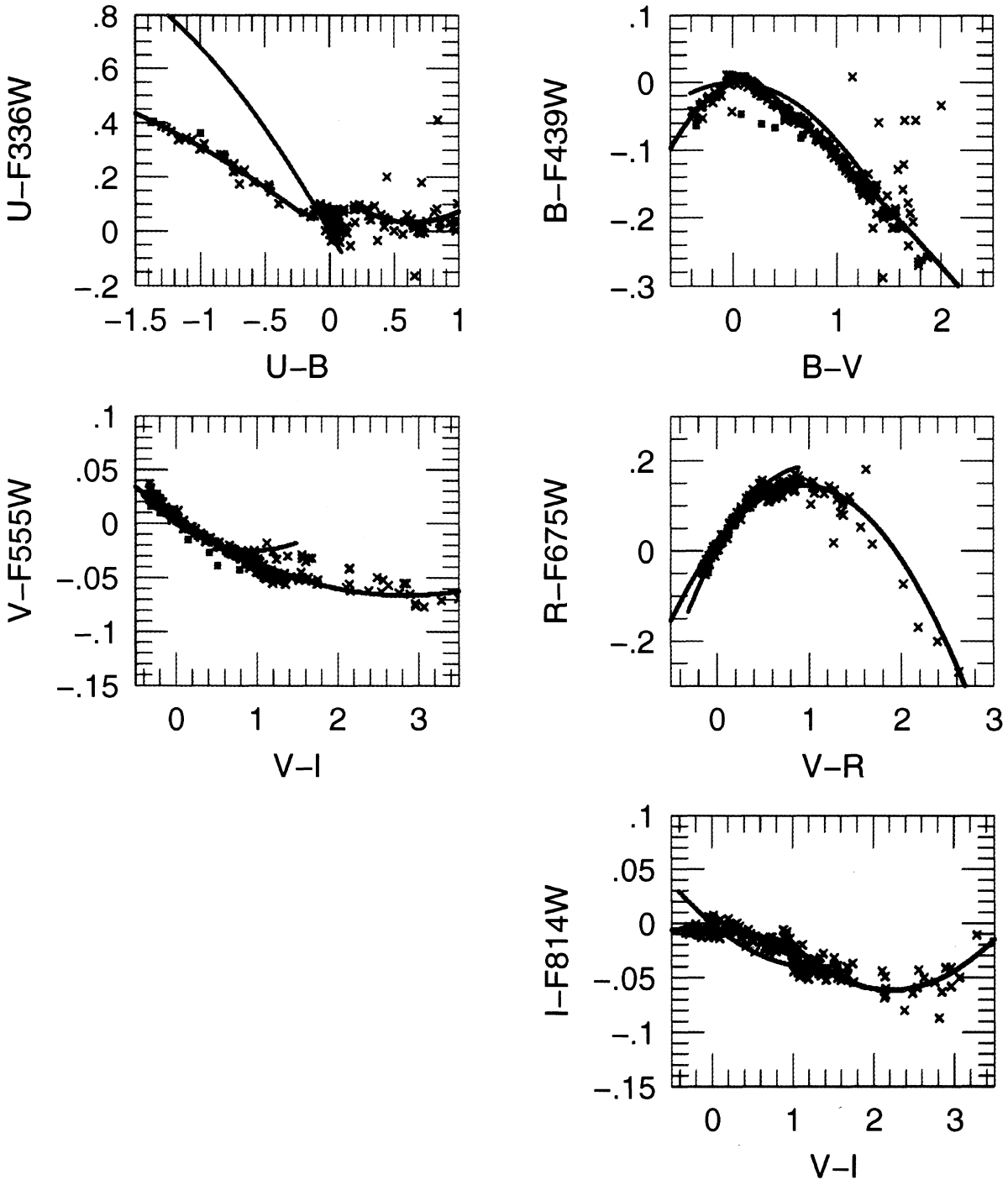

FIG. 9—Synthetic WFPC2-to-*UBVRI* transformations from the BPGS stellar atlas for primary photometric filters. Crosses show the synthetic measurements for the BPGS atlas. The blue-filled points are synthetic results for the spectrophotometric standards which have higher surface gravity. The black line shows the synthetic transformation derived from the BPGS stars, and the red line shows the observed WFPC2-to-*UBVRI* transformation.

synthetic results for the BPGS spectra which are for both main-sequence stars and giants. The filled blue points show synthetic results for the spectrophotometric standards, which have higher surface gravity. The black lines are fits to the synthetic transformations, and the red lines are the flight-to-*UBVRI* transformations derived from Secs. 3 and 4 and presented in Table 7. Some differences are expected between these transformations and the BPGS sequence because the observed transformations apply to stars of high surface gravity at high temperature and low surface gravity at low temperature, while the BPGS spectra do not sample high surface gravities (because the BPGS are bright, so hot main-

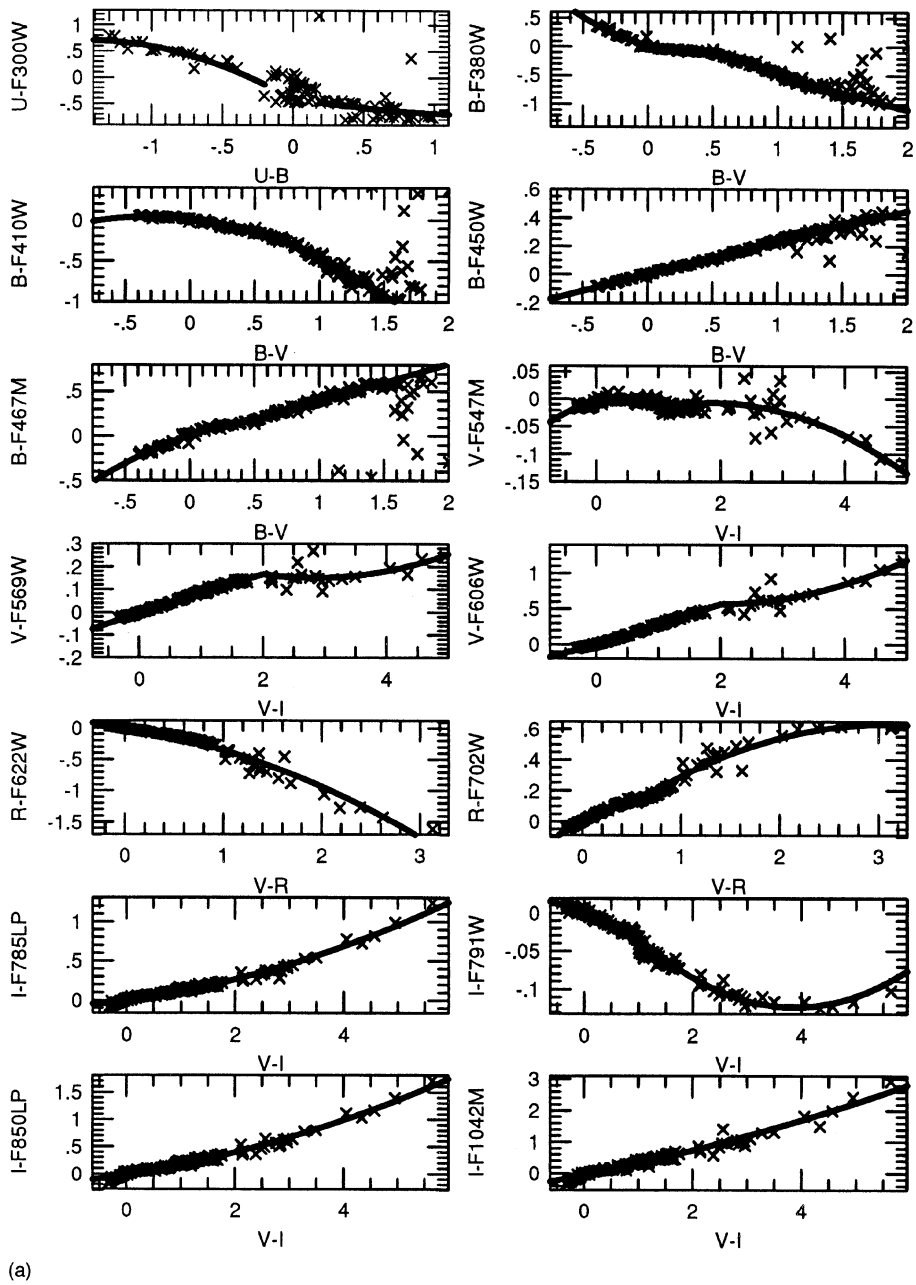

FIG. 10—(a) Synthetic WFPC2-to-*UBVRI* transformations for other filters. Crosses show the synthetic measurements from the BPGS atlas. The line shows the transformations derived from the synthetic results, which are presented in Table 10.

sequence stars are included, while white dwarfs are not). The largest deviations arising from surface gravity are in the F336W and F439W transformations, as discussed in Sec. 6.

Figure 9 shows that the synthetic system seems to match observations fairly well, within a couple of percent for all stars within the range of colors in which our observations were made. The situation is significantly worse for F336W, but we believe that this is likely caused by the problems with the *U*-band synthetic magnitudes. The shape of the observed transformation in F814W seems to be significantly different from that defined by the BPGS sequence, although the difference between the two never gets larger than about two percent. This suggests that the shape of either the *I* or the F814W passbands is incorrect. Since we cannot tell which is in error and since the deviations of the synthetic results from the observed ones are not especially large, we have chosen not to make any modifications to improve the match. However, we think it is more likely that the *I* curve is in error; if we use the Bessell curve for the *I* passband, we get better agreement with the observed transformation. The difference between the observed and synthetic transformation in F439W is well explained by the different sampling of surface

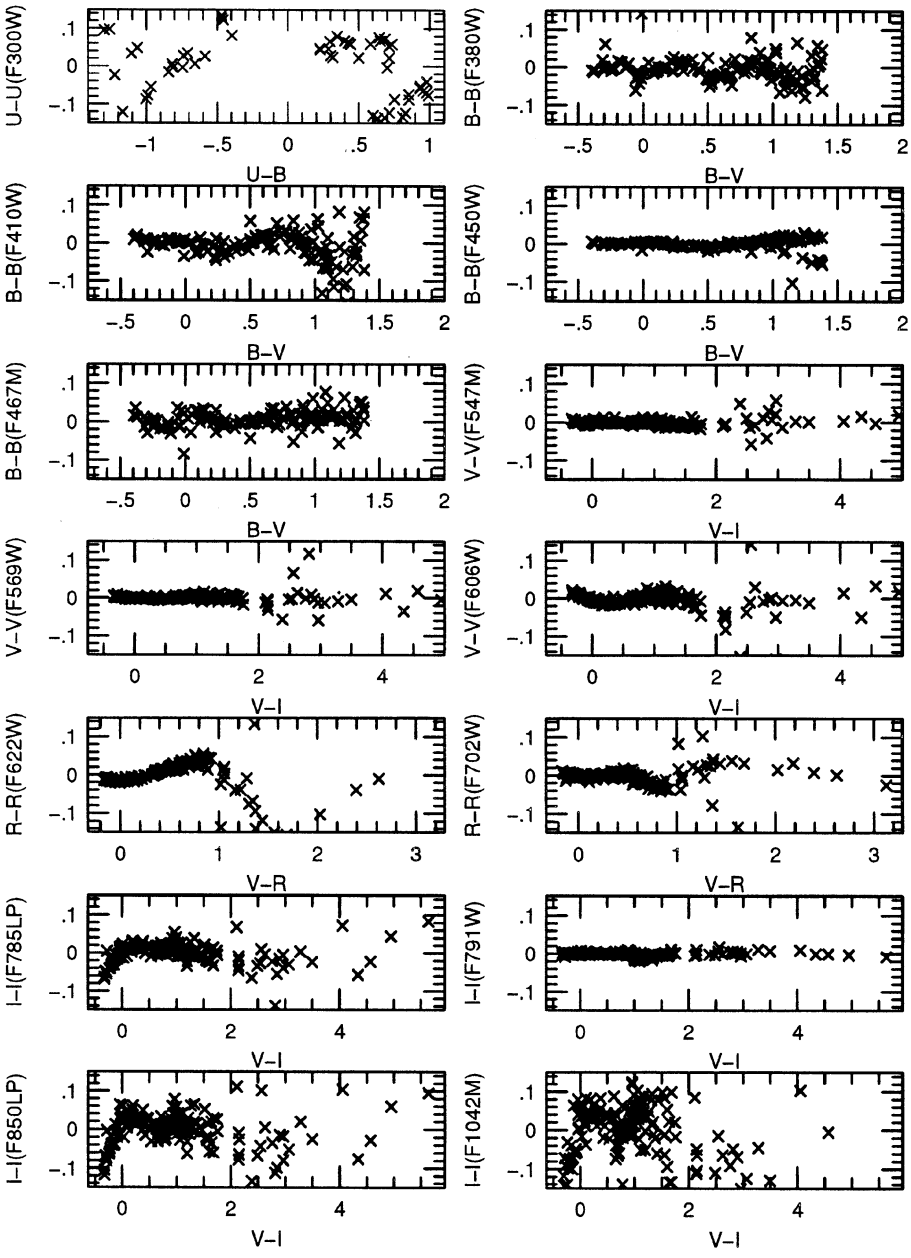

FIG. 10— (b) Residuals of synthetic photometry from the transformations shown in(a) and presented in Table 10.

gravities for stars around color zero. Note that the apparent discrepancy between the observed and synthetic transformation for F555W amounts to only a few percent for the reddest stars observed from the ground, and that, in fact, the observed transformation is not all that well constrained for these stars (see Fig. 4).

This analysis suggests that we have a reasonably good understanding of the WFPC2 synthetic system. The response curves give transformations which are likely to be accurate to a couple of percent or better in all visible filters except F336W. The synthetic curves can thus be used to extend to the transformations to objects with spectra different from the observed standards. In addition, we use the synthetic results to derive transformations for all filters in which we have not made ground-based calibration observations.

The derived synthetic transformations from the entire BPGS library for all of the visible medium and broad-band WFPC2 filters are shown in Figs. 9 (primary photometric filters) and Fig. 10(A) (other photometric filters) and are presented in Table 10. We have added the synthetic zero points to the derived transformations from the BPGS library so all transformations are of the form:

TABLE 10
Synthetic Transformations from WFPC2 System to UBVRI[a]

Filter	SMAG	SCOL	T_1	T_2	Z	C_{min}	C_{max}
F336W[b]	U	(U-B)	-0.382±0.065	-0.055±0.040	18.524±0.024	···	-0.2
	U	(U-B)	-0.389±0.331	0.306±0.266	18.696±0.094	0.2	1.0
F439W	B	(B-V)	0.056±0.047	-0.173±0.062	20.044±0.005	···	0.2
	B	(B-V)	-0.132±0.011	-0.010±0.011	20.078±0.000	0.2	1.4
F555W	V	(V-I)	-0.051±0.001	0.009±0.000	21.729±0.001	···	···
F675W	R	(V-R)	0.182±0.005	-0.097±0.002	21.249±0.002	···	···
F814W	I	(V-I)	-0.006±0.010	-0.012±0.004	20.838±0.001	···	1.0
	I	(V-I)	-0.124±0.003	0.028±0.001	20.920±0.000	1.0	···
F300W[b]	U	(U-B)	-1.532±0.379	-0.519±0.234	18.156±0.142	···	-0.2
	U	(U-B)	-0.427±0.807	0.138±0.649	18.181±0.229	0.2	1.0
F380W	B	(B-V)	-0.581±0.086	0.777±0.062	20.144±0.012	···	0.5
	B	(B-V)	-0.943±0.107	0.103±0.088	20.496±0.000	0.5	1.4
F410M	B	(B-V)	-0.183±0.037	-0.287±0.033	18.815±0.011	···	1.4
F450W	B	(B-V)	0.230±0.006	-0.003±0.006	21.175±0.002	···	1.4
F467M	B	(B-V)	0.480±0.067	-0.299±0.048	19.167±0.010	···	0.5
	B	(B-V)	0.432±0.144	-0.002±0.118	19.118±0.000	0.5	1.4
F547M	V	(V-I)	0.027±0.008	-0.032±0.003	20.834±0.001	···	1.1
	V	(V-I)	0.049±0.005	-0.013±0.001	20.786±0.000	1.1	···
F569W	V	(V-I)	0.089±0.006	-0.003±0.001	21.417±0.002	···	2.0
	V	(V-I)	-0.125±0.026	0.022±0.005	21.749±0.000	2.0	···
F606W	V	(V-I)	0.254±0.015	0.012±0.003	22.093±0.005	···	2.0
	V	(V-I)	-0.247±0.067	0.065±0.014	22.883±0.000	2.0	···
F622W	R	(V-R)	-0.252±0.015	-0.111±0.007	21.557±0.006	···	···
F702W	R	(V-R)	0.343±0.022	-0.177±0.015	21.633±0.002	···	0.6
	R	(V-R)	0.486±0.020	-0.079±0.009	21.511±0.000	0.6	···
F785LP	I	(V-I)	0.091±0.004	0.020±0.001	19.880±0.003	···	···
F791W	I	(V-I)	-0.029±0.006	-0.004±0.002	20.707±0.001	···	1.0
	I	(V-I)	-0.084±0.002	0.011±0.001	20.748±0.000	1.0	···
F850LP	I	(V-I)	0.160±0.007	0.023±0.002	19.122±0.005	···	···
F1042M[c]	I	(V-I)	0.350±0.015	0.022±0.004	15.314±0.012	···	···

[a]These coefficients should be used with the transformation given by Eq. (9). As discussed in the text, the quoted zero points refer to 0".5 radius aperture measurements after correction for CTE effects.

[b]The synthetic transformations for F300W and F336W are likely to be significantly in error because of inaccuracies in the assumed *U* filter curve. For F336W, we recommend the use of the observed transformation in Table 7 or that observers work in the WFPC2 system. For F300W, we recommend that observers work in the WFPC2 system.

[c]The shape of the system response curve longward of 1 micron has significant uncertainties, so it is possible that the derived transformation could have significant errors.

$$\mathrm{SMAG} = -2.5\times\log(\mathrm{DN\ s^{-1}}) + T_{1,FS,\mathrm{syn}}\times\mathrm{SCOL} + T_{2,FS,\mathrm{syn}} \times\mathrm{SCOL}^2 + Z_{FS,\mathrm{syn}} + 2.5\ \log \mathrm{GR}_i \quad (9)$$

where SMAG and SCOL are the standard magnitude and color, $T_{1,FS,\mathrm{syn}}$ and $T_{2,FS,\mathrm{syn}}$ are the synthetic flight-to-*UBVRI* transformation coefficients, $Z_{FS,\mathrm{syn}}$ is the zero point, and GR_i is the gain ratio.

Because of the large color range spanned by the stellar atlas, a single second-order transformation did not fit the entire range for all of the filters. The last columns in Table 10 give the range over which the fits were made, and multiple fits in different ranges are tabulated for several filters. Even these multiple second-order fits did not adequately represent the transformations well for some of the filters. Figure 10(B) shows the residuals of the synthetic magnitudes from the transformations presented in Table 10, so observers can assess the accuracy of the fits for any particular color.

For F336W and F300W, no attempt was made to make a fit for $-0.2<(U-V)<0.2$ because the transformations are double-valued in this regime. In any case, the synthetic transformations from these filters to the *U* filter are likely to have significant errors arising from errors in our assumed *U* filter curve. Observers with F336W data are advised to use the observed transformation in Table 7; for F300W, we advise observers not to transform, but to work entirely within the WFPC2 system.

The errors in the coefficients in Table 10 were derived by assuming equal weights for all of the synthetic points, then scaling the derived errors by the observed scatter. As such, these errors are probably dominated by errors arising from different transformations for stars with different spectral details. The errors in the zero point do not include estimates of errors in the derived response curve; such errors probably add an additional 1%–2% systematic error.

Transformations in Table 10 are presented for only one choice of standard color to save space. However, it is straightforward to make fits for arbitrary choice of standard color, and fits for other choices are available upon request.

5.4 Calibration of UV Filters

Since there are no well-established photometric systems in the UV, we have chosen a slightly different approach to presenting the UV photometric calibration. In Table 11, we present estimated effective wavelengths of the UV filters for a variety of unreddened model spectra of different temperatures. The models are from Kurucz (1993) for temperatures less than 20,000 K (solar metallicity, $\log g=5$) and from Bergeron (private communication) for DA white-dwarf models with $T\geqslant 20{,}000$ ($\log g=7$). We also present monochromatic fluxes, $F_{\lambda 0}$, at these wavelengths, which correspond to

TABLE 11
UV Calibration Data

	F160W		F170W		F185W		F218W		F255W		F300W	
T	λ_e	$F_{\lambda 0}$	λ_e	$F_{\lambda 0}$	λ_e	$F_{\lambda 0}$	λ_e	$F_{\lambda 0}$	λ_e	$F_{\lambda 0}$	λ_e	$F_{\lambda 0}$
5000	1491	1.517E-17	1747	4.985E-19	1954	4.416E-17	2189	5.226E-16	2588	5.722E-16	2951	7.270E-17
6000	1491	5.274E-17	1747	3.407E-17	1954	8.291E-16	2189	2.950E-15	2588	8.175E-16	2951	1.311E-16
7000	1491	1.148E-16	1747	1.319E-15	1954	4.243E-15	2189	2.895E-15	2588	9.818E-16	2951	1.367E-16
8000	1491	3.804E-16	1747	3.302E-15	1954	4.984E-15	2189	2.531E-15	2588	1.141E-15	2951	1.378E-16
9000	1491	6.783E-15	1747	4.180E-15	1954	5.072E-15	2189	2.391E-15	2588	1.203E-15	2951	1.371E-16
10000	1491	1.534E-14	1747	3.707E-15	1954	4.973E-15	2189	2.340E-15	2588	1.215E-15	2951	1.360E-16
20000	1491	1.371E-14	1747	3.507E-15	1954	4.702E-15	2189	2.236E-15	2588	1.173E-15	2951	1.327E-16
30000	1491	1.322E-14	1747	3.470E-15	1954	4.676E-15	2189	2.236E-15	2588	1.171E-15	2951	1.319E-16
40000	1491	1.310E-14	1747	3.478E-15	1954	4.684E-15	2189	2.233E-15	2588	1.170E-15	2951	1.317E-16
50000	1491	1.304E-14	1747	3.466E-15	1954	4.676E-15	2189	2.227E-15	2588	1.165E-15	2951	1.313E-16
60000	1491	1.299E-14	1747	3.453E-15	1954	4.672E-15	2189	2.228E-15	2588	1.165E-15	2951	1.312E-16
70000	1491	1.302E-14	1747	3.450E-15	1954	4.683E-15	2189	2.222E-15	2588	1.168E-15	2951	1.311E-16
80000	1491	1.294E-14	1747	3.442E-15	1954	4.676E-15	2189	2.225E-15	2588	1.167E-15	2951	1.308E-16
90000	1491	1.290E-14	1747	3.437E-15	1954	4.669E-15	2189	2.225E-15	2588	1.165E-15	2951	1.314E-16
100000	1491	1.287E-14	1747	3.435E-15	1954	4.667E-15	2189	2.226E-15	2588	1.164E-15	2951	1.310E-16

a count rate of 1 DN (gain=14) s^{-1} for the tabulated spectra. These can be used to convert observed count rates to monochromatic fluxes at the effective wavelengths using:

$$F_\lambda(\lambda_e)=(\mathrm{DN\ s^{-1}})/\mathrm{GR}_i\times F_{\lambda 0}, \quad (10)$$

where $DN\ s^{-1}$ is the observed count rate, GR_i is the gain ratio, and $F_{\lambda 0}$ and λ_e are taken from Table 11. Users are cautioned that these models are not guaranteed to be a good match to real objects, especially for the cooler stars, and also that the tabulated effective wavelengths and flux conversions will be incorrect for reddened sources. For careful UV calibration, users are advised to obtain the system and filter response curves and derive their own calibration using spectral models and extinction curves.

For surface photometry, the procedure to convert to fluxes is the same, except the system throughputs need to be increased by ~10% to correct the response to "infinite" aperture (see Sec. 2.5). This corresponds to lowering the fluxes in Table 11 by ~10%.

The UV calibration is significantly more uncertain than the visible calibration for several reasons. There are variations in response from chip to chip, and possibly within a chip, which may not be removed by flat fielding, as discussed in Sec. 2.3. There is variable contamination at UV wavelengths. Finally, the derived system response curve in the UV is significantly more uncertain than in the visible. These combined effects could give several tens of percent error in the UV calibration.

5.5 Calibration of Narrow-band Filters

The narrow-band filters are most often used for observations of emission-line objects. Observed count rates can be converted into physical fluxes using the throughput of the *HST*/WFPC2 system at the wavelength at which the object emits for narrow lines, or by calculating the product of the line profile and the throughput curve for broader lines. The peak throughputs for the narrow-band filters which generally, though not always, correspond closely to the throughput at the rest wavelength of the prominent emission line which the filter was designed to cover, are presented in Table 8 under the heading $q_{\max}$. These have been derived from the synthetic WFPC2 system. To convert observed count rates to physical fluxes, one simply uses

$$F=(\mathrm{DN\ s^{-1}}\times 14/\mathrm{GR}_i)\times E/(A\times QT), \quad (11)$$

where F is the total flux in the line, $E=hc/\lambda$ is the energy of a photon at the wavelength of the line, $A=\pi R^2$ where R is the radius of the *HST* primary (120 cm), and QT is the system throughput at the wavelength of the line.

For precise narrow-band calibration, it is important to get the throughput at the wavelength of the emission line. Consequently, it may be necessary to closely inspect the response curve for the particular filter to get the transmission at the correct wavelength rather than just using the $q_{\max}$ value from Table 8, especially if the object is red or blue shifted. Also, for the narrow-band filter calibration, errors in the derived response curve will translate directly into errors in the fluxes, since the filter scaling which was done to match continuum sources may be in error. Consequently, narrow-band calibration is probably accurate only to with ~5%, and possibly worse for filters at the extreme wavelengths or filters for which we did not have data to estimate revised filter scalings, e.g., for F343N, F375N, F390N, and F953N.

For surface photometry, the procedure to convert to fluxes is the same, except the system throughputs need to be increased by ~10% to correct the response to "infinite" aperture (see Sec. 2.5).

6. TRANSFORMATION SENSITIVITIES TO SPECTRAL DETAILS

We can use the synthetic system to investigate dependences of transformations on metallicity, gravity, or reddening. Similarly we can investigate whether objects with composite spectra, e.g., galaxies, transform differently from stars. Since we do not have spectrophotometric data for many different types of objects, we use the model atmospheres of Kurucz (1993) to investigate these dependences. Model atmospheres are known to have some problems in matching observations (e.g., Worthey 1994), but we are interested here only in differential effects and it is unlikely that these will be affected by small errors in the spectra. Similarly, minor errors in the response curves for either the WFPC2 or the *UBVRI* synthetic systems are unlikely to cause significant trouble.

Figure 11 presents synthetic transformations between the WFPC2 and *UBVRI* synthetic systems as a function of synthetic *UBVRI* color. The three different point types and colors represent three different metallicities: [Fe/H]=0 (black triangles), [Fe/H]=−1.0 (pink squares), and [Fe/H]=−2.0 (green circles). For each point type, multiple surface gravities are plotted; the surface gravities from Kurucz range from log g=5.0 down to about the minimum gravity for which a model in hydrostatic equilibrium exists. To sample higher gravities, appropriate for white dwarfs, points from the model spectra of Bergeron (private communication) are included (purple crosses). Filled points (blue squares) represent data for synthetic "galaxy" spectra, which are created by combining multiple stellar models (Worthey 1994); these spectra are single burst integrated models, with ages of 8, 12, and 17 Gyr. The "galaxy" spectra are shown for three redshifts of z=0, 0.5, and 1.0. The red triangles show the solar metallicity Kurucz points, but with a reddening of $E(B-V)$ =0.5 applied.

These figures show that the dependences of the transformations on various quantities are typically a few percent, except for U-F336W, where the sensitivity to surface gravity and reddening can be quite large. Gravity provides the largest spread for stars around color zero, while metallicity causes more spread for redder stars. The differences in magnitudes between white dwarfs and main-sequence stars for stars of color zero are very consistent with the observed difference in the synthetic zero points (tied to Vega) and the observed zero points (tied to white dwarfs), as presented in Table 9. The presence of reddening errors can render transformations less accurate especially for the transformations which depart significantly from linear relations. The transformations for galaxies, especially at high redshifts, can depart

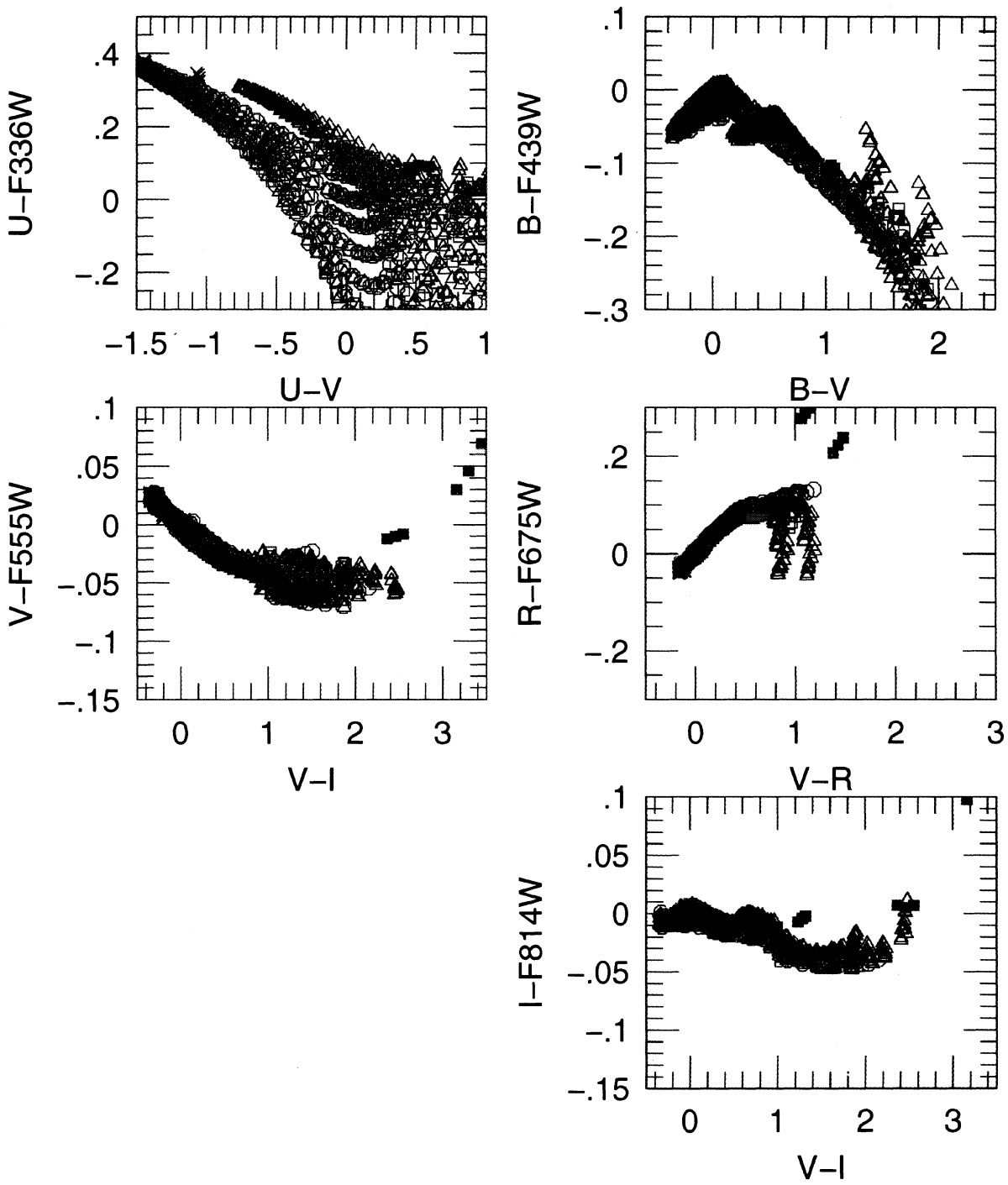

FIG. 11—Synthetic WFPC2-to-*UBVRI* transformations from model atmospheres for the primary photometric filters. Black triangles are for solar metallicity, purple squares are [Fe/H]=−1, and green circles are [Fe/H]=−2 (all from Kurucz); different points at the same color represent different surface gravities. The blue crosses are for white-dwarf models (Bergeron). The blue-filled squares are integrated single-burst models (Worthey) and represent "galaxy" spectra for ages of 8, 12, and 17 Gyr at redshifts of z=0,0.5,1.

strongly from the relations derived from stellar spectra.

We conclude that transformations from the WFPC2 system to *UBVRI* can be applied to most stellar observations without introducing errors of more than a few percent depending on the details of the spectra of the stars being observed. However, one cannot apply transformations and be guaranteed to preserve 2% accuracy. In F336W, transformations are highly dependent on surface gravity and reddening

and must be used with extreme caution, if at all. Transforming WFPC2 observations of galaxies to *UBVRI* should be done with caution, and probably not for high redshift objects. In general, we recommend working within the WFPC2 system when possible, and always carefully considering possible systematic errors in transformations when transforming WFPC2 magnitudes to *UBVRI*.

7. REDDENING IN THE WFPC2 SYSTEM

The WFPC2 filters have significantly different bandpasses than *UBVRI* filters, and this is important when making reddening corrections. Even if good transformations exist between the systems, a reddening correction in transformed *UBVRI* will be incorrect because the WFPC2 filters have different effective wavelengths. It is important to make reddening corrections in the WFPC2 system *before* transforming to *UBVRI*.

Figure 12 presents a plot of extinction for several WFPC2 filters and for *UBVRI* as a function of $E(B-V)$ up to $E(B-V)=1.0$. Tables 12(a) and 12(b) have the same data for the WFPC2 filters and also includes significantly higher reddenings. These data were computed synthetically using the extinction law presented in Cardelli et al. (1989), who parametrize interstellar extinction by the quantity $R_V \equiv A(V)/E(B-V)$; we adopted a value of $R_V=3.1$. Because the WFPC2 bandpasses are wide, there can be differences in extinction depending on the stellar color; in Fig. 12, solid lines were computed with an O6 input spectrum and the dotted line was computed with a K5 spectrum (both from the BPGS atlas).

Figure 12 shows that the extinction in F439W and F555W is systematically higher than in B and V because these WFPC2 filters have shorter effective wavelengths than B and V. The strong dependence of F336W extinction on stellar color arises because F336W extends far into the UV, where extinction changes rapidly with wavelength. Also, as mentioned previously, F336W has a fairly significant red leak, and when the extinction gets larger, the red leak becomes more important; this is obvious in Table 12 at extremely high

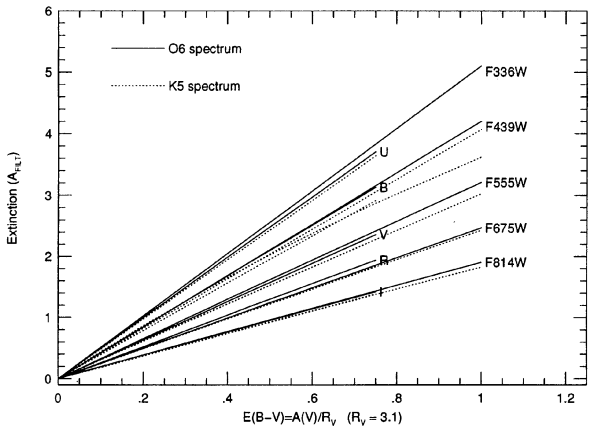

FIG. 12—Extinction in WFPC2 filters and *UBVRI* as a function of $E(B-V)$ from synthetic results using interstellar extinction curve from Cardelli et al. (1989)

TABLE 12
(a) Extinction in Primary WFPC2 Filters, O6 Spectrum.

E(B-V)	A_{F336W}	A_{F439W}	A_{F555W}	A_{F675W}	A_{F814W}
0.000	0.000	0.000	0.000	0.000	0.000
0.050	0.257	0.211	0.162	0.124	0.096
0.100	0.513	0.424	0.326	0.249	0.196
0.150	0.767	0.638	0.489	0.374	0.293
0.200	1.023	0.845	0.653	0.496	0.386
0.250	1.280	1.055	0.813	0.623	0.487
0.300	1.536	1.266	0.977	0.744	0.582
0.350	1.792	1.477	1.136	0.867	0.678
0.400	2.048	1.686	1.301	0.990	0.772
0.450	2.304	1.897	1.460	1.114	0.865
0.500	2.560	2.108	1.619	1.244	0.961
0.550	2.814	2.319	1.780	1.360	1.056
0.600	3.069	2.528	1.942	1.487	1.151
0.650	3.328	2.738	2.101	1.610	1.246
0.700	3.578	2.948	2.260	1.733	1.340
0.750	3.833	3.158	2.419	1.857	1.434
1.000	5.102	4.204	3.210	2.471	1.904
1.250	6.366	5.245	3.996	3.082	2.368
1.500	7.618	6.287	4.769	3.699	2.832
1.750	8.850	7.323	5.538	4.305	3.282
2.000	10.050	8.360	6.301	4.913	3.740
2.250	11.198	9.391	7.059	5.519	4.186
2.500	12.265	10.416	7.807	6.122	4.630
2.750	13.229	11.445	8.552	6.724	5.070
3.000	14.072	12.468	9.288	7.325	5.503
3.250	14.813	13.481	10.023	7.924	5.937
3.500	15.475	14.492	10.753	8.520	6.365
3.750	16.089	15.499	11.472	9.114	6.789
4.000	16.670	16.490	12.193	9.707	7.208
4.250	17.230	17.468	12.908	10.298	7.623
4.500	17.782	18.422	13.614	10.886	8.034
4.750	18.328	19.345	14.321	11.477	8.446

TABLE 12
(b) Extinction in Primary WFPC2 filters, K5 Spectrum

E(B-V)	A_{F336W}	A_{F439W}	A_{F555W}	A_{F675W}	A_{F814W}
0.000	0.000	0.000	0.000	0.000	0.000
0.050	0.221	0.205	0.154	0.122	0.094
0.100	0.440	0.407	0.309	0.245	0.183
0.150	0.651	0.610	0.462	0.367	0.275
0.200	0.865	0.820	0.614	0.489	0.368
0.250	1.065	1.023	0.767	0.611	0.461
0.300	1.267	1.224	0.919	0.733	0.553
0.350	1.463	1.429	1.070	0.855	0.645
0.400	1.656	1.632	1.224	0.977	0.737
0.450	1.843	1.837	1.375	1.098	0.829
0.500	2.025	2.040	1.523	1.221	0.920
0.550	2.204	2.244	1.680	1.340	1.012
0.600	2.379	2.448	1.827	1.462	1.102
0.650	2.548	2.650	1.977	1.584	1.194
0.700	2.711	2.854	2.129	1.705	1.284
0.750	2.872	3.057	2.278	1.829	1.376
1.000	3.620	4.071	3.026	2.431	1.825
1.250	4.289	5.081	3.765	3.036	2.276
1.500	4.906	6.089	4.507	3.635	2.715
1.750	5.493	7.092	5.233	4.237	3.154
2.000	6.063	8.088	5.958	4.831	3.588
2.250	6.621	9.081	6.680	5.431	4.019
2.500	7.175	10.061	7.395	6.027	4.443
2.750	7.721	11.031	8.105	6.618	4.869
3.000	8.265	11.975	8.813	7.214	5.285
3.250	8.809	12.893	9.518	7.799	5.702
3.500	9.348	13.774	10.215	8.387	6.113
3.750	9.883	14.590	10.912	8.974	6.523
4.000	10.415	15.341	11.599	9.555	6.926
4.250	10.943	16.023	12.289	10.142	7.326
4.500	11.466	16.625	12.972	10.724	7.729
4.750	11.982	17.168	13.651	11.303	8.127

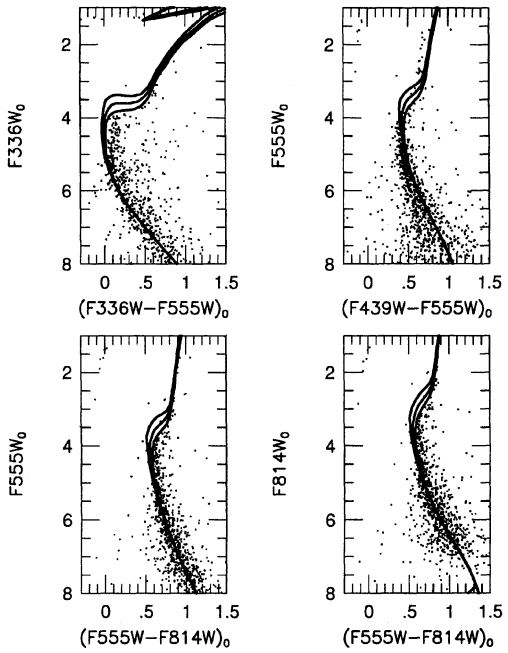

FIG. 13—Color–magnitude diagrams for ω Cen. Observations have been converted to absolute magnitudes and unreddened colors using data in text. Solid lines show isochrones for ages of 12, 15, and 18 Gyr.

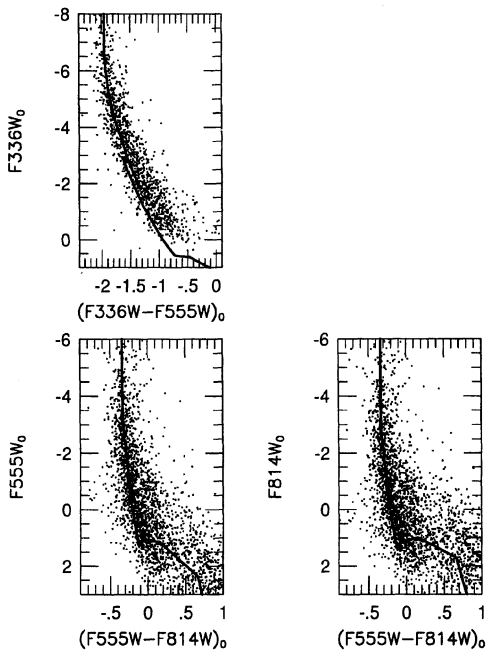

FIG. 15—Color–magnitude diagrams for R136. Observations have been converted to absolute magnitudes and unreddened colors using data in text. Solid lines show isochrones for an age of 4 Myr.

reddenings, where the extinction in F439W exceeds that in F336W!

Extinction curves for arbitrary spectra and values of R_V can be computed using the WFPC2 synthetic system response curves and an assumed interstellar extinction curve.

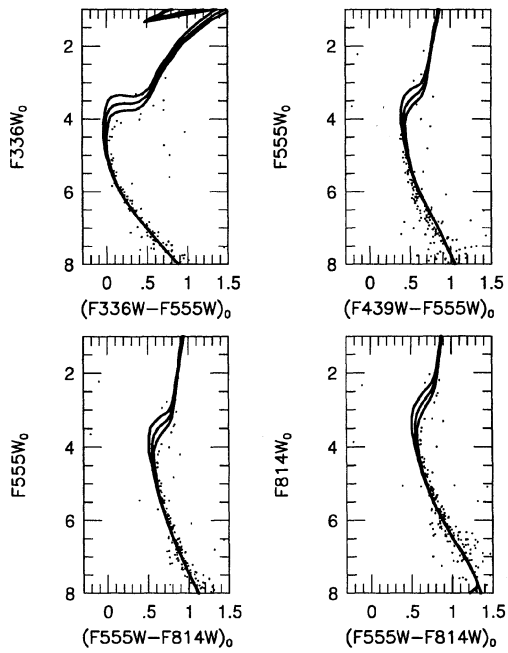

FIG. 14—Color–magnitude diagrams for NGC 6752. Observations have been converted to absolute magnitudes and unreddened colors using data in text. Solid lines show isochrones for ages of 12, 15, and 18 Gyr.

8. ISOCHRONES IN THE WFPC2 SYSTEM

Using the synthetic WFPC2 system, we can take physical quantities from stellar models and transform them into the observational plane. We have constructed a set of WFPC2 system isochrones using the stellar models of Vandenberg and collaborators (Vandenberg 1985; Vandenberg and Bell 1985; Vandenberg and Laskarides 1987) and the Revised Yale Isochrones (Green et al. 1987), as compiled by Worthey (1994). These provide stellar interior models which we have coupled to the model stellar atmospheres of Kurucz (1993). To get absolute magnitudes we have set the bolometric correction of the Sun to be -0.12 and adopted a solar M_V=4.72, following Worthey (1994). These data, in conjunction with the response curves, can be used to give synthetic WFPC2 magnitudes for a population with given metallicity and age.

To check the accuracy of the calibration, we have taken isochrones and matched them to observed sequences in ω Cen, NGC 6752, and R136. Unfortunately, this checks the calibration only to the extent to which the stellar models and atmospheres are correct. In fact, determining accurate stellar models is very difficult, and this section just provides a estimate to how well observations can be matched with this set of models.

Data for ω Cen and NGC 6752 were measured using aperture photometric from the calibration dataset, while the R136 data was measured using PSF-fitting photometry on some early WFPC2 observations (Hunter et al. 1995). For all clusters, data was put on the WFPC2 synthetic system using the synthetic zero points from Table 9.

We have taken distances and reddenings from the literature for these clusters. For ω Cen, we use $(m-M)_0$=13.5,

$E(B-V)=0.11$, [Fe/H]$=-1.57$; for NGC 6752, $(m-M)_0=12.9$, $E(B-V)=0.04$, [Fe/H]$=-1.61$ (W. Harris, private communication). For R136, we started by using $(m-M)_0=18.55$, $E(B-V)=0.38$, [Fe/H]$=-0.3$, (Hunter et al. 1995), but we adjusted the reddening to $E(B-V)=0.43$ to get the best match with the data; this is on the high end of previous estimates of reddening towards R136. We converted the reddenings to extinctions in the WFPC2 passbands as discussed in Sec. 6, with $R_V=3.1$ for ω Cen and NGC 6752, and $R_V=3.4$ for R136.

Figures 13, 14, and 15 present these data along with isochrones. For ω Cen and NGC 6752, isochrones for ages 12, 15, and 18 Gyr are shown; for R136, isochrones from Schaerer et al. (1993) for the high-mass stars and from Swenson (private communication) for the low-mass stars are shown for an age of 4 Myr and 1/2 solar metallicity. The isochrone fits vary in quality. For ω Cen and NGC 6752, the fits are good in F555W and F814W except around the turnoff and in the subgiant branch. There are larger mismatches in F336W and F439W. In R136, the matches are fairly good for all colors.

Both ω Cen and NGC 6752 have similar mismatches in the isochrones. No zero-point shift in any of the colors would allow a good match between the isochrones and the data. Consequently, we believe that either the stellar isochrone or atmosphere data are likely to be in error for these clusters, with significant mismatches found in F336W and F439W. This is perhaps not surprising, as it is difficult to model cool stellar atmospheres in the blue. The mismatch around the turnoff is F555W and F814W cannot be easily explained by errors in zero point, distance, or reddening; it would be of interest to compare independent stellar isochrone or atmosphere data with the observations. We note that the isochrones here assume scaled solar abundances for all heavy elements and do not include the effects of diffusion. Still, other observers have derived better matches using comparable ages for other globular clusters with these same isochrones; we are slightly distressed that we don't seem to be able to get a better match, but this currently does not appear to be a calibration problem.

To confirm this, we computed *BVRI* colors from the Kurucz atmospheres with the same stellar interior models and compared these isochrones with the observed *BVRI* magnitudes in ω Cen from Walker (1994); this procedure is totally independent of any WFPC2 calibration. This comparison showed very similar mismatches between the observed and model data, strongly suggesting that calibration is not the cause of the less than perfect isochrone matches discussed above in the WFPC2 system.

In R136, hot stars are sampled which probably have less uncertainties in the stellar atmospheres. It is very encouraging for photometric calibration to see a good match between the isochrones and data!

9. A PHOTOMETRIC CALIBRATION COOKBOOK

Here we briefly summarize the steps required to calibrate photometry for a WFPC2 image.

9.1 Point-Source Photometry in the Visible

(1) Reduce the image using the prescription in H95 or use the STScI pipeline reduced image.

(2) Consider a CTE correction. If there is negligible background in the frame (less than a few dozen electrons), CTE problems are probably present. At higher background levels, the problems are probably significantly reduced, though some stars may still be affected. Remember that the CTE effect depends on the CCD temperature, and use the correction appropriate to the CCD temperature (which changed from -76 to -88 °C on 1994 April 23). You may wish to contact the STScI Instrument Scientists to find out if more information on CTE effects is available.

(3) Perform photometry of objects in the field, using aperture photometry, PSF-fitting photometry, etc. This should give a set of measurements in units of DN s^{-1} for all of your objects. If you didn't correct the image for CTE effects, consider correcting the photometry.

(4) Correct the photometry for geometric distortion effects to normalize observed count rates to what they would be in the center of WF3 (see Sec. 2.3.1).

(5) Determine the offset between your photometry and aperture photometry with a 0.″5 radius aperture. Probably this will be done by measuring a few bright, relatively uncrowded objects in the field. Apply this offset to all of the photometric measurements.

(6a) If you are observing continuum sources and want to work in the synthetic WFPC2 system, e.g., if you want to compare your observations with model predictions from isochrones, etc., convert the observed count rates to instrumental magnitudes ($m=-2.5\times\log(\mathrm{DN/s^{-1}})$) and add the photometric zero point listed in Table 9. If your observations are made with gain=7, add the constant $2.5\times\log \mathrm{GR}_i$.

(6b) If you are observing continuum sources and want to transform to *UBVRI*, convert to instrumental magnitudes. If you are using one of the primary photometric filters and your objects are not very red, use the observed transformations given by Eq. (8) with the coefficients in Table 7. If you are using another filter or have objects outside the color range of the observed standard stars, use the synthetic transformations [Eq. (9) and Table 10]. You may wish to make a correction for interstellar extinction before applying the transformations. You will need to have made observations in more than one color, or else will need to have an estimate of the color of your object in the *UBVRI* system to be able to apply the correct color terms. Remember the gain-ratio term if your observations are made with gain=7.

(6c) If you are observing emission-line point sources, determine the system throughput (QT) through your filter at the wavelength of the emission line. The observed flux is then given by Eq. (11).

For any of (6a), (6b), or (6c), remember that you should add ~0.05 to the photometric zero points in the near IR if your data was taken before 1994 April 23 (at a CCD temperature of -76 °C), to account for the higher near-IR QE when the CCDs were warmer.

9.2 Surface Photometry in the Visible

(1) Reduce the image using the prescription in H95 or use the STScI pipeline reduced image.

(2) Consider a CTE correction (see point 2 in Sec. 9.1).

(3) Measure surface brightnesses in units of DN/s/area.

(4a) To convert to WFPC2 magnitudes/square arcsec, convert the count rates to instrumental magnitudes per square arcsec (see H95 to get the pixel scales). Use Eq. (7) with the observed zero points from Table 7 or the synthetic zero points from Table 9. Add a constant of approximately 0.1 mag to correct the zero points to infinite aperture (see Sec. 2.5 and H95).

(4b) To convert to UBVRI magnitudes/square arcsec, convert the count rates to instrumental magnitudes per square arcsec. Use the transformation relations given by Eq. (8) with the coefficients presented in Table 7 (observed transformations for primary filters) or those given by Eq. (9) with the coefficients in Table 10 (synthetic transformations). Add a constant of approximately 0.1 mag to each zero point to correct to infinite aperture (see Sec. 2.5 and H95).

(4c) To convert to fluxes per square arcsec for emission-line sources, convert the count rates to counts per square arcsec. Determine the system throughput (QT) through your filter at the wavelength of the emission line. Multiply the system throughput by ~1.1 to correct to infinite aperture. The observed flux is then given by Eq. (11).

9.3 Photometry in the UV

(1) Reduce the image using the prescription in H95 or use the STScI pipeline reduced image.

(2) Consider a CTE correction (see point 2 in Sec. 9.1).

(3) Measure integrated or surface brightnesses.

(4) Correct for geometric distortion if measuring integrated brightnesses.

(5) Choose a model spectrum from Table 11. Use Eq. (10) to convert the observed count rate to a monochromatic flux at the effective wavelength for this choice of input spectrum. You may wish to consider alternate spectra to those in Table 11, e.g., spectra with reddening. If this is the case, obtain the system and filter response curves and convolve them with your desired spectra to derive fluxes and effective wavelengths.

10. CONCLUSIONS

We have discussed the photometric performance and calibration of WFPC2. Photometric performance is affected by CTE effects, contamination, and the accuracy of flat fields.

CTE effects currently probably give the largest uncertainties for photometry in the visible. For moderately bright stars with little background at the current CCD temperature of −88 °C, the effect has a maximum amplitude of ~4% for 0.″5 radius aperture photometry and can probably be characterized to within a percent or two. For scenes with background, the effect is likely to be smaller, based on laboratory experiments. CTE losses for very faint stars in scenes with little background or for the wings of brighter stars have not been well characterized, though some observations suggest that these losses may not be significantly larger than for brighter stars. The detailed effect of CTE losses as a function of brightness and background level is being determined from additional calibration observations.

The accumulation of contaminants on the cold CCD windows affects throughput in the UV. Monthly decontaminations when the CCDs are warmed for several hours restore the throughput completely. The rate of throughput degradation varies from chip to chip, but it seems repeatable over decontamination cycles, so a correction can be applied with is probably accurate to a few percent. We have determined and presented such corrections. Significant variations in contamination across each chip may also exist.

Flat fields are good to a few percent in the visible region of the spectrum. There appear to be significant differences in response in the UV between the four different channels which are not corrected by the flat fields. These may represent different levels of permanent contamination in the different channels.

Photometric calibration data have been obtained for the primary photometric filters which provide transformations from WFPC2 observations to *UBVRI* magnitudes and to physical fluxes. Both a WFPC2 ground photometric system and a WFPC2 flight photometric system have been defined. The ground observations allow the determination of accurate transformations to *UBVRI* and consequently, of well-defined zero points. The transformations between the flight and the ground WFPC2 systems have been determined from observations of a few calibration fields. These allow an accurate definition of the WFPC2 flight photometric system, and transformations between this system and *UBVRI*.

A WFPC2 synthetic system has been constructed which reproduces observed count rates of spectrophotometric standards to within 1%–2%. Using the synthetic system, zero points and flux conversions have been derived for all of the WFPC2 filters. Synthetic results give transformations between all of the photometric filters and *UBVRI*. These transformations match the observed transformations fairly accurately after differences in the definition of the two systems are taken into account for all filters except F336W; for this filter, we believe the synthetic transformation disagrees because of errors in the *U*-band synthetic photometry, not errors in the F336W synthetic results. The synthetic system consists of a system response curve and filter transmission curves which are available from STScI.

Transformations to *UBVRI* are dependent on details of the stellar spectra, and should be used with caution. The dependences have been investigated using the synthetic system on model atmospheres. Generally, transformed data will be accurate to within a few percent, but differences can be significantly larger for the *U* and *B* bands or for peculiar spectra. The effective wavelengths of the WFPC2 filters can differ significantly from their *UBVRI* counterparts, so accurate reddening corrections must be made in the WFPC2 system, not in transformed magnitudes. Extinction curves for the primary WFPC2 filters for a standard interstellar reddening law have been presented, and extinction for other filters or reddening

laws can be derived using the synthetic WFPC2 system.

The WFPC2 synthetic system can be used to construct isochrones. Comparison of isochrones with some observed data shows no obvious calibration errors in the synthetic system.

The process of understanding and calibrating WFPC2 is ongoing. In particular, several calibration proposals have been devised to attempt to get a better understanding of some of the problems discussed in this paper, e.g., CTE losses and the accuracy of the flat fields. Observers are encouraged to keep posted for future reports from the STScI which may have new information, and to contact the Instrument Scientists with questions. Requests for additional calibration observations are welcomed by the STScI, although with a limited amount of time available for calibration, all such observations must generally be prioritized along with other calibration needs.

Note added in proof: Several observers have reported that observations of the same field with different exposure times (e.g., 60 and 1200 s) appear to have zero points differing by up to 0.05 mag, in the sense that the longer exposures have higher count rates. It is not clear whether the effect occurs in all observations, and no good physical explanation for this effect has been proposed. If the effect is real, then the photometric calibration presented in this paper may give systematic errors if applied to long exposures, since all of the observations described here were made with short exposure times. This phenomenon is still under investigation, and observers are encouraged to consult with the StScI WFPC2 Instrument Group to get the latest information and advice.

Many people have contributed to this work. In particular, we thank Arlo Landolt for providing unpublished magnitudes and data relating to the *UBVRI* system, Luis Colina for useful discussions about synthetic photometry, Robert Kurucz for providing a CDROM with stellar atmosphere models, Hugh Harris for useful suggestions, and Peter Stetson for carefully looking at photometric results and discussing them. We thank the WF/PC and WFPC2 Investigation Definition Teams, in particular Ed Groth for careful consideration of issues and Bill Baum for guiding WF/PC calibration over the last decade. The personnel at STScI have written many of the calibration proposals, made useful comments, and were always available to confirm and discuss results. Finally, we are indebted to the staff at Siding Springs Observatory for making the ground observations possible with our CCD system and for making our trip to Australia pleasant and productive. This work was supported in part by NASA under Contract No. NAS7-918 to JPL and subcontract 959145 from JPL to Lowell Observatory, and in part by NASA through Grant No. HF-1066.01-94A from the Space Telescope Science Institute, which is operated by AURA, Inc., under NASA Contract No. NAS5-26555.

REFERENCES

Bessell, M. F. 1990, PASP, 102, 1181
Bohlin, R. C., Harris, A. W., Holm, A. V., and Gry, C. 1990, ApJS, 73, 413
Bruzual, Persson, Gunn, Stryker stellar atlas, from the STScI database
Cardelli, J. A., Clayton, G. C., and Mathis, J. S. 1989, ApJ, 345, 245
Colina, L., and Bohlin, R. C. 1994, AJ, 108, 1931
Green, E. M., Demarque, P., and King, C. R. 1987, The Revised Yale Isochrones and Luminosity Functions (New Haven, Yale University Observatory)
Harris, H. C., Baum, W. A., Hunter, D. A., and Kreidl, T. J. 1991, AJ, 101, 677
Harris, H. C., Hunter, D. A., Baum, W. A., and Jones, J. H. 1993, AJ, 105, 1196
Hayes, D. S. 1985, Calibration of Fundamental Stellar Quantities, IAU Symposium No. 111, ed. D. S. Hayes, L. E. Pasinetti, and A. G. D. Phillip (Dordrecht, Reidel), p. 225
Holtzman, J. A., Hester, J. J., Casertano, S., Trauger, J. T., Watson, A. M., and The WFPC2 IDT 1995, PASP, 107, 156 (H95)
Hunter, D. A., Shaya, E. J., Holtzman, J. A., Light, R. M., and O'Neil, Jr., E. J. 1995, ApJ (in press)
Krist, J., and Burrows, C. J. 1994, WFPC2 Instrument Science Report, STScI
Kurucz, R. L. 1992, private communication to G. Worthey
Kurucz, R. L. 1993, ATLAS9 Stellar Atmosphere Programs and 2 km/s grid, CD-ROM 13, Smithsonian Astrophysical Observatory
Landolt, A. U. 1973, AJ, 78, 959
Landolt, A. U. 1983, AJ, 88, 439
Landolt, A. U. 1992a, AJ, 104, 340
Landolt, A. U. 1992b, AJ, 104, 72
Oke, J. B. 1990, AJ, 99, 1621
Schaerer, D., Meynet, G., Maeder, A., and Schaller, G. 1993, AAS, 98, 523
Stetson, P. B. 1987, PASP, 99, 191
Stetson, P. B. 1992, JRASC, 86, 71
VandenBerg, D. A. 1985, ApJS, 58, 711
VandenBerg, D. A., and Bell, R. A. 1985, ApJS, 58, 561
Vandenberg, D. A., and Laskarides, P. G. 1987, ApJS, 64, 103
Walker, A. R. 1994, PASP, 106, 828
Worthey, G. 1994, ApJS, 95, 107